Electronic Supplementary Material (ESI) for Green Chemistry.

Biotransformation of C20- and C22-polyunsaturated fatty acids and fish oil hydrolyzates to *R*,*R*-dihydroxy fatty acids as lipid mediators by double-oxygenating 15*R*-lipoxygenase

Jin Lee,[a] Yoon-Joo Ko,[b] Jin-Byung Park,[c] and Deok-Kun Oh*[,a]

[a]*Department of Bioscience and Biotechnology, Konkuk University, Seoul 05029, Republic of Korea.*

[b]*National Center for Inter-University Research Facilities (NCIRF), Seoul National University, Seoul 08826, Republic of Korea.*

[c]*Department of Food Science and Engineering, Ewha Woman's University, Seoul 03760, Republic of Korea.*

***Corresponding Author**

E-mail: deokkun@konkuk.ac.kr; Fax: +82-2-444-5518; Tel: +82-2-454-3118; ORCID: 0000-0002-6886-7589

Table of Contents

Supporting Tables

Table S1. Primer design for amplification of specific DNA sequences 5
Table S2. Regression equations for calibration curves of PUFAs, MonoHFAs, and DiHFAs 7
Table S3. Docking energy and distance of ARA (**1**) from 10 LOXs existed in *S. cellulosum* 8
Table S4. Specific activities of double-oxygenating LOXs from mouse, *Endozoicomonas numazuensis*, *Archangium violaceum*, and *S. cellulosum* 9
Table S5. 1D NMR data of 5*R*,15*R*-DiHETE (**4**) in MeOD (850 MHz NMR) 10
Table S6. 1D NMR data of 5*R*,15*R*-DiHEPA (**8**) in MeOD (850 MHz NMR). 11
Table S7. 1D NMR data of 7*R*,17*R*-DiHDHA (**12**) in MeOD (850 MHz NMR). 12

Supporting Figures

Fig. S1. Alignment of the amino acid sequences of 10 putative LOXs in *S. cellulosum* 13
Fig. S2. Reverse-phase HPLC profiles of MonoHFAs obtained from the conversion of ARA (**1**) by the selected 6 LOXs derived from *S. cellulosum* with standard. 14
Fig. S3. 15*R*-LOX sequence derived from *S. cellulosum* so ce1871. 15
Fig. S4. Normal-phase HPLC profiles of MonoHFAs obtained from the conversion of ARA (**1**) by the selected 3 LOXs derived from *S. cellulosum* with HETE standards. 17
Fig. S5. Chiral-phase HPLC profiles of MonoHFAs obtained from the conversion of ARA (**1**) by the selected 3 putative LOXs derived from *S. cellulosum* (UniProtKB protein numbers, A0A2LESS6, A0A2L0ESU2, and S4XZS0) with 9*S*-, 9*R*-, 12*S*-, 12*R*-, 15*S*-, and 15*R*-HETE (**3**) standards. 18
Fig. S6. Reverse- and chiral-phase HPLC profiles of the reaction products obtained from the conversion of ARA (**1**) by the putative LOX cloned with the primer of S4XZS0 with standards. 20
Fig. S7. SDS-PAGE analysis and gel filtration chromatography of *S. cellulosum* 15*R*-LOX expressed in *E. coli* C2566. 22

Fig. S8. Effects of temperature and pH on the production of 15*R*-HETE (**3**) from ARA (**1**) by 15*R*-LOX from *S. cellulosum*.....23
Fig. S9. LC-MS/MS profiles of MonoHFA and DiHFA obtained from the conversion of ARA (**1**) by 15*R*-LOX from *S. cellulosum*.....24
Fig. S10. LC-MS/MS profiles of MonoHFA and DiHFA obtained from the conversion of EPA (**5**) by 15*R*-LOX from *S. cellulosum*. 25
Fig. S11. LC-MS/MS profiles of MonoHFA and DiHFA obtained from the conversion of DHA (**9**) by 15*R*-LOX from *S. cellulosum*. 26
Fig. S12. Normal-phase HPLC profiles of DiHFA obtained from the conversion of ARA (**1**) by *S. cellulosum* 15*R*-LOX with 5*R*,15*S*-DiHETE, 5*S*,15*R*-DiHETE, 5*S*,15*S*-DiHETE, and 5*R*,15*R*-DiHETE (**4**) standards. 27
Fig. S13. ^{1}H NMR and ^{13}C NMR peaks of 5*R*,15*R*-DiHETE (isomer of leukotriene B4; **4**) in deuterated methanol (MeOD) (850 MHz NMR).....28
Fig. S14. 2D NMR data of 5*R*,15*R*-DiHETE (**4**) in MeOD (850 MHz NMR).....29
Fig. S15. ^{1}H NMR and ^{13}C NMR peaks of 5*R*,15*R*-DiHEPA (enantiomer of resolvin E4; **8**) in MeOD (850 MHz NMR). 30
Fig. S16. 2D NMR data of 5*R*,15*R*-DiHEPA (**8**) in MeOD (850 MHz NMR).....31
Fig. S17. ^{1}H NMR and ^{13}C NMR peaks of 7*R*,17*R*-DiHDHA (enantiomer of resolvin D5; **12**) in MeOD (850 MHz NMR). 32
Fig. S18. 2D NMR data of 7*R*,17*R*-DiHDHA (**12**) in MeOD (850 MHz NMR). 33
Fig. S19. Effects of temperature and pH on the biotransformation of ARA (**1**) into 5*R*,15*R*-DiHETE (**4**) by *E. coli* expressing 15*R*-LOX from *S. cellulosum* 34
Fig. S20. Optimization of cell and substrate concentrations for the biotransformation of ARA (**1**) into 5*R*,15*R*-DiHETE (**4**) by *E. coli* expressing 15*R*-LOX from *S. cellulosum*.....35
Fig. S21. Optimization of cell and substrate concentrations for the biotransformation of ARA (**1**) into 5*R*,15*R*-DiHETE (**4**) by *E. coli* expressing 15*R*-LOX from *S. cellulosum* at the optimal ratio of cells to substrate. 36
Fig. S22. Binding of absorbent resins to ARA (**1**) as a substrate. 37
Fig. S23. Effect of resin SP825 concentration on the biotransformation of ARA (**1**) into 5*R*,15*R*-DiHETE (**4**) by 15*R*-LOX from *S. cellulosum* with varying the concentrations of cells and ARA (**1**). 38
Fig. S24. Biotransformation of PUFAs into DiHFAs with the addition of resin by *E. coli* expressing 15*R*-LOX from *S. cellulosum* in filtrate. 39
Fig. S25. Biotransformation of PUFAs into DiHFAs with the addition of resin by *E. coli* expressing 15*R*-LOX from *S. cellulosum* in resin. 41
Fig. S26. Reliability of the models of 15*R*-LOX from *S. cellulosum* built by Alphafold and Discovery studio (DS).....43

Fig. S27. Confirmation of the active site in 15*R*-LOX from *S. cellulosum* in DS model by Alphafold model.....45
Fig. S28. Reverse-phase HPLC profiles of the products obtained from the conversion of ARA (**1**) by the wild-type and variant LOXs at position 354 from *S. cellulosum*.....46
Fig. S29. Reverse-phase HPLC profiles of the products obtained from the conversions of ARA (**1**) and 15*R*-HETE (**3**) by the wild-type and variant LOXs at position 606 from *S. cellulosum*.....47
Fig. S30. Effects of temperature and pH on the biotransformation of ARA (**1**) into 15*R*-HETE (**3**) by *E. coli* expressing 15*R*-LOX from *S. cellulosum*. ..48
Fig. S31. Effects of cell and substrate concentration on the biotransformation of ARA (**1**) into 15*R*- HETE (**3**) by *E. coli* expressing engineered 15*R*-LOX (L606F variant). 51
Fig. S32. Optimization of cell and substrate concentration on the biotransformation of ARA (**1**) into 15*R*- HETE (**3**) by *E. coli* expressing engineered 15*R*-LOX (L606F variant) 52

References **53**

Supporting Tables

Table S1 Primer design for amplification of specific DNA sequences[a]

UniprotKB	Name	Restriction enzyme	Sequence (5'→3')
S4XZS0	pET28a-SCLOX-F (LOX)	*Nde* I	AGCGGCCTGGTGCCGCGCGGCAGCCATATG ATGAGTAACCCGTCCCTGCCTCAAAACGAC
	pET28a-SCLOX-R (LOX)	*Nde* I	GTGGTGGTGCTCGAGTGCGGCCGCAAGCTT TCAGATGTTGATGCTCTGCGGGATCTGCGA
	pET28a-SCLOX-F (Vector)	*Hind* III	TCGCAGATCCCGCAGAGCATCAACATCTGA AAGCTTGCGGCCGCACTCGAGCACCACCAC
	pET28a-SCLOX-R (Vector)	*Hind* III	GTCGTTTTGAGGCAGGGACGGGTTACTCATC ATATGGCTGCCGCGCGGCACCAGGCCGCT
A0A150S935	pET28a-F (LOX)	*Nde* I	AGCGGCCTGGTGCCGCGCGGCAGCCATATG ATGAGCCTGTTCGACGTTCCGGTCCTGCCG
	pET28a-R (LOX)	*Nde* I	ATCTCAGTGGTGGTGGTGGTGGTGCTCGAGT CAGATATTGATGCTCTGCGGGATGGCCGA
	pET28a-F (Vector)	*Xho* I	TCGGCCATCCCGCAGAGCATCAATATCTGA CTCGAGCACCACCACCACCACCACTGAGAT
	pET28a-R (Vector)	*Xho* I	CGGCAGGACCGGAACGTCGAACAGGCTCAT CATATGGCTGCCGCGCGGCACCAGGCCGCT
A0A150QTF6	pET28a-F (LOX)	*Nde* I	AGCGGCCTGGTGCCGCGCGGCAGCCATATG[a]ATGAGCCTGTTCGACGTTCCGGTCCTGCCG
	pET28a-R (LOX)	*Nde* I	GTGGTGGTGCTCGAGTGCGGCCGCAAGCTT TCAGATATTGATGCTCTGCGGGATGGCCGA
	pET28a-F (Vector)	*Hind* III	TCGGCCATCCCGCAGAGCATCAATATCTGA AAGCTT[a]GCGGCCGCACTCGAGCACCACCA C
	pET28a-R (Vector)	*Hind* III	CGGCAGGACCGGAACGTCGAACAGGCTCAT CATATGGCTGCCGCGCGGCACCAGGCCGCT
A0A4P2Q3W5	pET28a-F (LOX)	*Nde* I	AGCGGCCTGGTGCCGCGCGGCAGCCATATG ATGAGGTACCCCTCTCTGCCGCAGAAGGAC
	pET28a-R (LOX)	*Nde* I	GTGGTGGTGCTCGAGTGCGGCCGCAAGCTT TCAGATGTTGATGCTCTGGGGGATCTGGGA
	pET28a-F	*Hind* III	TCCCAGATCCCCCAGAGCATCAACATCTGA

	(Vector)		AAGCTTGCGGCCGCACTCGAGCACCACCAC
	pET28a-R (Vector)	*Hind* III	GTCCTTCTGCGGCAGAGAGGGGTACCTCAT CATATGGCTGCCGCGCGGCACCAGGCCGCT
A0A2L0ESS6	pET28a-F (LOX)	*Nde* I	AGCGGCCTGGTGCCGCGCGGCAGCCATATG ATGGGGGCATTGATGACAGTCGACTACAAG
	pET28a-R (LOX)	*Nde* I	GTGGTGGTGCTCGAGTGCGGCCGCAAGCTT TCAGATGGTGATTCCGCAGGGGATCTTGTC
	pET28a-F (Vector)	*Hind* III	GACAAGATCCCCTGCGGAATCACCATCTGA AAGCTTGCGGCCGCACTCGAGCACCACCAC
	pET28a-R (Vector)	*Hind* III	CTTGTAGTCGACTGTCATCAATGCCCCCATC ATATGGCTGCCGCGCGGCACCAGGCCGCT
A0A2L0ESU2	pET28a-F (LOX)	*Nde* I	AGCGGCCTGGTGCCGCGCGGCAGCCATATG ATGCTCGCCGCGCTGCGCCGCCTGTTATCG
	pET28a-R (LOX)	*Nde* I	GTGGTGGTGCTCGAGTGCGGCCGCAAGCTT TCAGATGTTGATTCGGGACTGCACCGTCCT
	pET28a-F (Vector)	*Hind* III	AGGACGGTGCAGTCCCGAATCAACATCTGA AAGCTTGCGGCCGCACTCGAGCACCACCAC
	pET28a-R (Vector)	*Hind* III	CGATAACAGGCGGCGCAGCGCGGCGAGCAT CATATGGCTGCCGCGCGGCACCAGGCCGCT

[a] The restriction sites are underlined.

Table S2 Regression equations for calibration curves of PUFAs, MonoHFAs, and DiHFAs[a,b]

Type	Compound	Regression equation[a]	r^2
PUFAs	**1**	$y = 0.0000358x - 0.0001$	0.9912
	5	$y = 0.0000301x + 0.0007$	0.9904
	9	$y = 0.0000277x - 0.0008$	0.9812
MonoHpFAs and MonoHFAs[b]	**2** and **3**	$y = 0.00009061x - 0.0008$	0.9812
	6 and **7**	$y = 0.000192x + 0.0015$	0.9761
	10 and **11**	$y = 0.0000688x - 0.0091$	0.9914
DiHFAs	**4**	$y = 0.0000751x - 0.0002$	0.9880
	8	$y = 0.00006181x + 0.0007$	0.9970
	12	$y = 0.00004814x + 0.00108$	0.9671

PUFAs, polyunsaturated fatty acid; MonoHFAs, hydroxy fatty acids; MonoHpFAs, Monohydroperoxy fatty acids; DiHFAs, dihydroxy fatty acids; ARA (**1**), arachidonic acid; EPA (**5**), eicosapentaenoic acid; DHA (**9**), docosahexaenoic acid; 15*R*-HpETE (**2**), 15*R*-hydroperoxy-5*Z*,8*Z*,11*Z*,13*E*-eicosatetraenoic acid; 15*R*-HpEPA (**6**), 15*R*-hydroperoxy-5*Z*,8*Z*,11*Z*,13*E*,17*Z*-eicosapentaenoic acid; 17*R*-HpDHA (**10**), 17*R*-hydroperoxy-4*Z*,7*Z*,10*Z*,13*Z*,15*E*,19*Z*-docosahexaenoic acid; 15*R*-HETE (**3**), 15*R*-hydroxy-5*Z*,8*Z*,11*Z*,13*E*-eicosatetraenoic acid; 15*R*-HEPA (**7**), 15*R*-hydroxy-5*Z*,8*Z*,11*Z*,13*E*,17*Z*-eicosapentaenoic acid; 17*R*-HDHA (**11**), 17*R*-hydroxy-4*Z*,7*Z*,10*Z*,13*Z*,15*E*,19*Z*-docosahexaenoic acid; 5*R*,15*R*-DiHETE (isomer of LTB4; **4**), 5*R*,15*R*-dihydroxy-6*E*,8*Z*,11*Z*,13*E*-eicosatetraenoic acid; 5*R*,15*R*-DiHEPA (enantiomer of RvE4; **8**), 5*R*,15*R*-dihydroxy-6*E*,8*Z*,11*Z*,13*E*,17*Z*-eicosapentaenoic acid; 7*R*,17*R*-DiHDHA (enantiomer of RvD5; **12**), 7*R*,17*R*-dihydroxy-4*Z*,8*E*,10*Z*,13*Z*,15*E*,19*Z*-docosahexaenoic acid. [a] *x*, peak area in the HPLC profile; *y*, molar concentration of standard (mM). [b] Data represent the mean ± SD (n = 3) values. MonoHFAs or MonoHpFAs were obtained from the conversion of PUFAs by *E. coli* expressing ARA15*R*-LOX from *S. cellulosum* with or without cysteine as a reducing agent, respectively. The concentrations of HFAs calibrated by the peak areas were the same as those of HpFAs.[1]

Table S3 Docking energy and distance of ARA (**1**) from 10 LOXs existed in *S. cellulosum*

UniprotKB	Length	Docking energy (kcal/mol), *E*	Distance (Å, δ)	*E*/ δ	Regio- and stereoselectivity
A0A150S935	703	-76.1	10.9	-6.9	ND[a]
A0A150QTF6	704	-104.4	11.2	-9.3	ND
S4XZS0	673	-157.6	7.5	-21.0	15*R*
A0A4P2Q3W5	673	-105.3	12.4	-8.5	ND
A0A4P2QUL1	673	+13.5	6.7	+2.0	ND
A0A2L0ESU2	687	-50.1	8.4	-5.9	12*S*
A0A150TEU6	673	+20.4	10.5	+1.9	ND
A0A150T884	673	+18.5	9.7	+1.9	ND
A0A150PUW0	673	+5.0	4.9	+1.0	ND
A0A2L0ESS6	680	-40.5	6.9	-5.8	9*S*

[a] ND, not detected. The blue-colored letters indicate negative docking energy values.

Table S4 Specific activities of double-oxygenating LOXs from mouse, *Endozoicomonas numazuensis*, *Archangium violaceum*, and *S. cellulosum*[a,b]

Oxygenation	Substrate	Specific activity (μmol/min/mg)			
		S. cellulosum 15*R*-LOX	*A. violaceum* 15*S*-LOX[2]	*E. numazuensis* 12*S*-LOX[3]	Mouse 8*S*-LOX[4]
First	**1**	505 ± 1.5	282 ± 1.5	286 ± 2.2	14.9 ± 0.01
Second	HETE	80.1 ± 2.2	67.6 ± 2.2	54.3 ± 1.4	0.098 ± 0.003

ARA (**1**), arachidonic acid. [a] Data were detected by measuring reaction solution from **1** as substrate using HPLC in absorbance at 234 nm or reaction solution from HFAs as substrates in absorbance at 270 nm.

[b] Data represent the means of three experiments, and error bars represent the standard deviation.

Table S5 1D NMR data of 5*R*,15*R*-DiHETE (**4**) in MeOD (850 MHz NMR)

C No.	1H (δ)	Multiplet	*J* (Hz)	Protons	^{13}C (δ)
1					177.7
2	2.32	t	7.36	2H	34.97
3	1.75-1.61	m		2H	22.33
4	1.59-1.51	m		2H	37.83
5	4.13	td	7.23, 6.93	2H	73.01
6	5.68	dd	15.09, 6.93	1H	137.93
7	6.583	dd	14.71, 10.95	1H	126.43
8	6.01	dd	10.96, 10.72	1H	129.7
9	5.39	dt	9.95, 7.54	1H	130.46
10	3.1	t	7.44	2H	27.5
11	5.38	dt	10.65, 7.42	1H	130.23
12	6.01	dd	10.96, 10.72	1H	129.77
13	6.56	dd	15.22, 10.91	1H	126.22
14	5.67	dd	15.22, 5.73	1H	138.31
15	4.10	td	6.46, 5.73	1H	73.4
16	1.56-1.45	m		2H	38.54
17	1.42-1.29	m		2H	26.43
18	1.36-1.26	m		2H	33.12
19	1.37-1.29	m		2H	23.85
20	0.91	t	6.71	3H	14.57

Table S6 1D NMR data of 5*R*,15*R*-DiHEPA (**8**) in MeOD (850 MHz NMR)

C No.	1H (δ)	Multiplet	*J* (Hz)	Protons	^{13}C (δ)
1					178.1
2	2.31	t	7.27	2H	35.2
3	1.75-1.61	m		2H	22.4
4	1.59-1.50	m		2H	37.9
5	4.15-4.11	m		1H	73.3
6	5.68	dd	14.87, 6.64	1H	138
7	6.57	dd	14.87, 11.04	1H	126.4
8	6	dd	12.03, 11.04	1H	129.7
9	5.41-5.35	m		1H	130.4
10	3.1	t	7.5	2H	27.5
11	5.41-5.35	m		1H	130.4
12	6.01	dd	12.24 10.74	1H	129.7
13	6.58	dd	14.99, 12.24	1H	126.4
14	5.69	dd	14.99, 6.80	1H	137.7
15	4.15-4.11	m		1H	73.3
16	2.34-2.25	m		2H	36.4
17	5.38-5.34	m		1H	125.6
18	5.49	dt	10.73, 7.17	1H	134.8
19	2.06	qd	7.51, 7.17	2H	21.8
20	0.96	t	7.51	3H	14.7

Table S7 1D NMR data of 7*R*,17*R*-DiHDHA (**12**) in MeOD (850 MHz NMR)

C No.	1H (δ)	Multiplet	*J* (Hz)	Protons	^{13}C (δ)
1					177.3
2	2.35-2.31	m		2H	35.1
3	2.35-2.31	m		2H	24.2
4	5.50-5.45	m		1H	131.2
5	5.50-5.45	m		1H	127.6
6	2.35-2.29	m	6.63	2H	36.4
7	4.16	td	6.63, 6.46	1H	73.2
8	5.7	dd	15.04, 6.46	1H	137.6
9	6.57	dd	15.04, 10.54	1H	126.4
10	6.01	t	10.54	1H	129.7
11	5.39-5.35	m		1H	130.4
12	3.09	t	7.59	2H	27.5
13	5.39-5.35	m		1H	130.4
14	6	dd	10.37	1H	129.7
15	6.58	dd	15.14, 10.37	1H	126.4
16	5.69	dd	15.14, 6.38	1H	137.6
17	4.14	td	6.63, 6.38	1H	73.3
18	2.32-2.25	m	6.63	2H	36.4
19	5.39-5.35	m		1H	125.6
20	5.50-5.45	m		1H	134.8
21	2.06	qd	7.55, 7.21	2H	21.8
22	0.96	t	7.55	3H	14.7

Supporting Figures

Fig. S1 Alignment of the amino acid sequences of 10 putative LOXs in *S. cellulosum*. The UniProtKB protein numbers of the LOXs are A0A150S935, A0A150QTF6, S4XZS0, A0A4P2Q3W5, A0A4P2QUL1, A0A2L0ESU2, A0A150TEU6, A0A150T884, A0A150PUW0, and A0A2L0ESS6. Red boxes indicate metal-binding residues (catalytic residues).

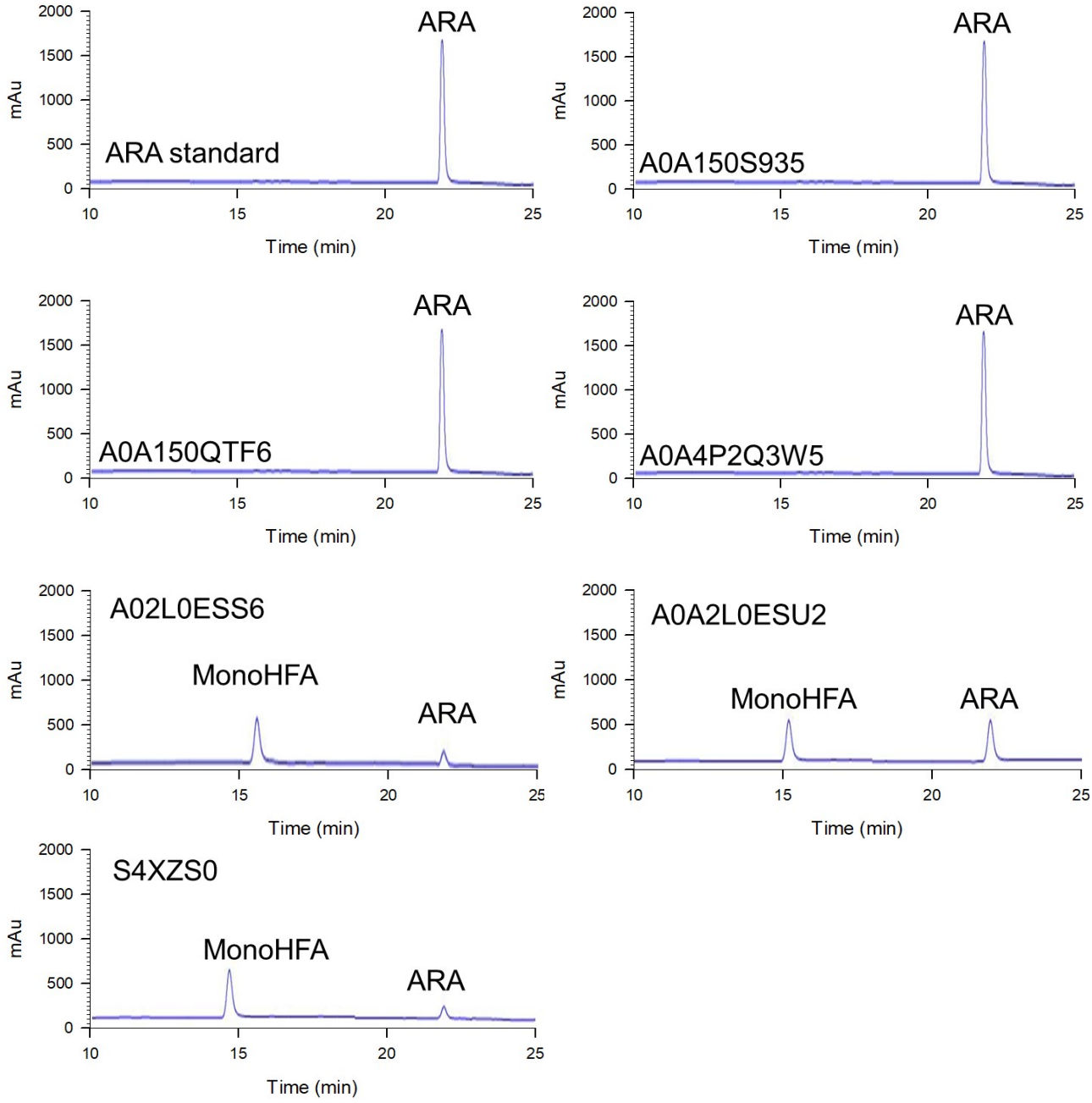

Fig. S2 Reverse-phase HPLC profiles of MonoHFAs obtained from the conversion of ARA (**1**) by the selected 6 LOXs derived from *S. cellulosum* with standard. The reactions were performed at 30 °C in 50 mM EPPS buffer (pH 8.0) containing 1.0 mM **1**, 0.1 g/L LOX, and 100 mM cysteine as reducing agent for 10 min. The peak area of **1** as substrate was not decreased by A0A150S935, A0A15QTF6, and A0A4P2Q3W5 proteins. However, A0A2LESS6, A0A2L0ESU2 and S4XZS0 proteins converted **1** into monoHFA.

A

```
New_15RLOX 1    MSNPSLPQNDSPAEQQQRKSELARAQQTYVYNHDTRLSPLGVAQSVPNGQGFAPILVGSA 60
                MSNPSLPQNDSPAEQQQRKSELARAQQTYVY+HDTRLSPLGVAQSVPNGQGFAPILVGSA
Template_S4XZS0 1    MSNPSLPQNDSPAEQQQRKSELARAQQTYVYDHDTRLSPLGVAQSVPNGQGFAPILVGSA 60

New_15RLOX 61   ALVILELVGNVVAKASKLVGSDGSLRSPKGAPLDEATSARIQGVLRDLKQRHRELTLALT 120
                ALVIL+LVGNVVAKASKLVGSDGSLRSPKGAPLD+ATSARIQGVL DLKQRHRELTL LT
Template_S4XZS0 61   ALVILDLVGNVVAKASKLVGSDGSLRSPKGAPLDDATSARIQGVLHDLKQRHRELTLVLT 120

New_15RLOX 121  PLHGEPERAPAPPPRPPAAALVEGFAQKFVATAENRVMESVLGAPNLSTKNVGDIIKSLL 180
                PLHGEPERAPAPPPR PA ALVEG AQKFV TAENR MESVLGA NLSTKNVGDIIKSLL
Template_S4XZS0 121  PLHGEPERAPAPPPRAPAVALVEGVAQKFVTTAENRAMESVLGATNLSTKNVGDIIKSLL 180

New_15RLOX 181  DTLLSAAGKLLLDLVGMYGQATSVYDYVSEFQTFRLPEIASAYQDDAIFAWMRVAGPNPL 240
                DTLLSAAGKLLLDLVGMYGQATSVYDYVSEFQTFRLPEIAS YQDDAIFAWMRVAGPNPL
Template_S4XZS0 181  DTLLSAAGKLLLDLVGMYGQATSVYDYVSEFQTFRLPEIASVYQDDAIFAWMRVAGPNPL 240

New_15RLOX 241  VLKRVASPGASFPVTDAQYRSVMGEGDSLASAGKEGRLYLADYEVLSQLVPGTAPDQQKY 300
                VLKRVASPGASFPVTDAQYRSVMGEGDSLASAGKEGRLYLADY+ LSQLVPGTAPDQQKY
Template_S4XZS0 241  VLKRVASPGASFPVTDAQYRSVMGEGDSLASAGKEGRLYLADYKALSQLVPGTAPDQQKY 300

New_15RLOX 301  VEAPLALFAVPAAGAPSRLLRPVAIQCAQAPGAASPIFTPSDGVAWEVAKLHVQVADGNF 360
                VEAPLALFAVPAAGAPSRLLRPVAIQCAQAPGAASPIFTPSDGVAWEVAKLHVQVADGNF
Template_S4XZS0 301  VEAPLALFAVPAAGAPSRLLRPVAIQCAQAPGAASPIFTPSDGVAWEVAKLHVQVADGNF 360

New_15RLOX 361  HELISHLGQTHLVMEAFAMATPRQLAPEHPVNVLLTPHFQGTLAINNAAEADLIAPGGPV 420
                HELISHLGQTHLV+EAFAMATPRQLAPEHPVNVLLTPHFQGTLAINNAAEADLIAPGGPV
Template_S4XZS0 361  HELISHLGQTHLVLEAFAMATPRQLAPEHPVNVLLTPHFQGTLAINNAAEADLIAPGGPV 420

New_15RLOX 421  DNLLAGTIASSTQLAVDAVLSYSVNQQFLPVALAHRGVDDPSALPSYPYRDDAVLLWGVI 480
                DNLLAGTIASSTQLAVDAVLSYSVNQQFLPVALA RGVDDPS LPSYPYRDDA LLWG I
Template_S4XZS0 421  DNLLAGTIASSTQLAVDAVLSYSVNQQFLPVALAQRGVDDPSTLPSYPYRDDATLLWGAI 480

New_15RLOX 481  HTWVSRYLAIYYTSDADVLGDYELQSWIAELSSPSECGLKDIGEDGAIRTVAYLTDLLTH 540
                HTWVSRYLA+YYTSDADVLGDYELQ WIAELSSPS CGLKDIGEDGAIRTVAYL DLLTH
Template_S4XZS0 481  HTWVSRYLAVYYTSDADVLGDYELQHWIAELSSPSGCGLKDIGEDGAIRTVAYLADLLTH 540

New_15RLOX 541  VVFTASAQHAAVNFPQSSLMSFTPALPLAAYAPAPSITAGLPSSEIFQHLPPLQQALLQL 600
                V+FTASAQHAAVNFPQSSLMSFTPALPLAAYAPAPSITAGLP SEIFQHLPPLQQALLQ+
Template_S4XZS0 541  VIFTASAQHAAVNFPQSSLMSFTPALPLAAYAPAPSITAGLPPSEIFQHLPPLQQALLQI 600

New_15RLOX 601  NVMMLLGGVYYSRLGDYDRNIPGAYFTDARVREPLEAFQRELMEIEATIGKRNLQRFPYL 660
                NVMMLLGGVYYSRLGDYDRNIPGAYFTDARVREPLEAFQRELMEIEATIGKRNLQRFPY+
Template_S4XZS0 601  NVMMLLGGVYYSRLGDYDRNIPGAYFTDARVREPLEAFQRELMEIEATIGKRNLQRFPYV 660

New_15RLOX 661  VLLPSQIPQSINI  673
                VLLPSQIPQSINI
Template_S4XZS0 661  VLLPSQIPQSINI  673
```

B

>*S. cellulosum*_15*R*_LOX

MSNPSLPQNDSPAEQQQRKSELARAQQTYVYNHDTRLSPLGVAQSVPNGQGFAPILVGSAALVILELVGNVVAKASKLVG

SDGSLRSPKGAPLDEATSARIQGVLRDLKQRHRELTLALTPLHGEPERAPAPPPRPPAAALVEGFAQKFVATAENRVMES

VLGAPNLSTKNVGDIIKSLLDTLLSAAGKLLLDLVGMYGQATSVYDYVSEFQTFRLPEIASAYQDDAIFAWMRVAGPNPL

VLKRVASPGASFPVTDAQYRSVMGEGDSLASAGKEGRLYLADYEVLSQLVPGTAPDQQKYVEAPLALFAVPAAGAPSRLL

RPVAIQCAQAPGAASPIFTPSDGVAWEVAKLHVQVADGNFHELISHLGQTHLVMEAFAMATPRQLAPEHPVNVLLTPHFQ

GTLAINNAAEADLIAPGGPVDNLLAGTIASSTQLAVDAVLSYSVNQQFLPVALAHRGVDDPSALPSYPYRDDAVLLWGVI

HTWVSRYLAIYYTSDADVLGDYELQSWIAELSSPSECGLKDIGEDGAIRTVAYLTDLLTHVVFTASAQHAAVNFPQSSLM

SFTPALPLAAYAPAPSITAGLPSSEIFQHLPPLQQALLQLNVMMLLGGVYYSRLGDYDRNIPGAYFTDARVREPLEAFQR

ELMEIEATIGKRNLQRFPYLVLLPSQIPQSINI

Fig. S3 15*R*-LOX sequence derived from *S. cellulosum* so ce1871. The sequence of this gene was not the same as that of the gene encoding S4XZS0, however, similar to the sequence. (A) Alignment of 15*R*-LOX from *S. cellulosum* so ce1871with the target protein sequence as S4XZS0 from *S. cellulosum* so ce56. (B) 15*R*-LOX sequence derived from *S. cellulosum* so ce1871.

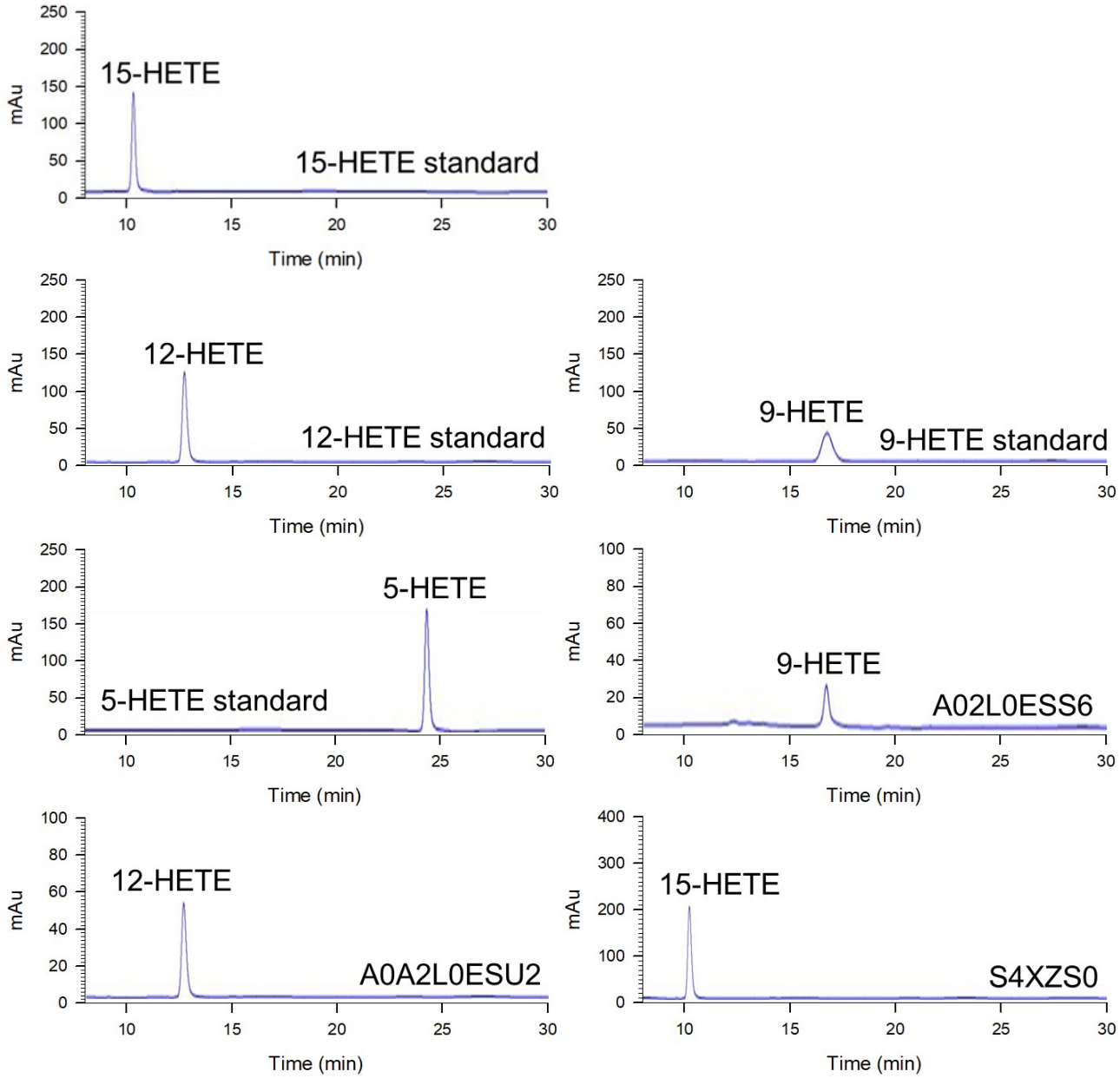

Fig. S4 Normal-phase HPLC profiles of MonoHFAs obtained from the conversion of ARA (**1**) by the selected 3 LOXs derived from *S. cellulosum* with HETE standards. HPLC profiles of the 15-, 12-, 9-, 5-HETE standards. HPLC profiles of the reaction products obtained from the conversion of ARA (**1**) by the selected 3 LOXs derived from *S. cellulosum*. The reaction products were analyzed with MonoHFA standards, including 15-, 12-, 9-, and 5-HETEs. The reactions were performed at 30 °C in 50 mM EPPS buffer (pH 8.0) containing 1.0 mM **1**, 0.1 g/L LOX, and 100 mM cysteine as reducing agent for 10 min. The reaction products of A0A2LESS6, A0A2L0ESU2, and S4XZS0 proteins were suggested as 9-, 12-, and 15-HETE, respectively.

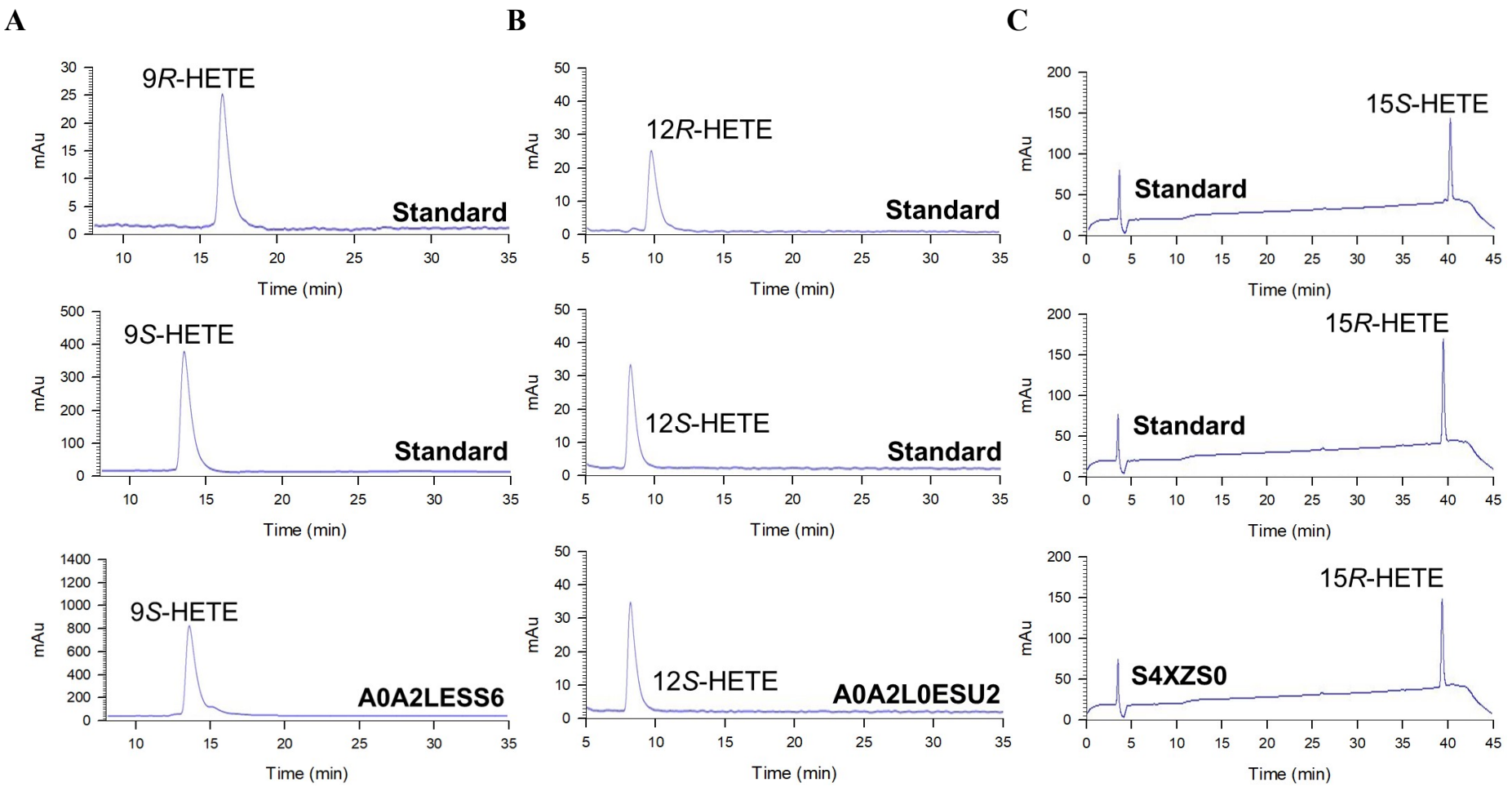
A
9R-HETE
Standard
9S-HETE
Standard
9S-HETE
A0A2LESS6
B
12R-HETE
Standard
12S-HETE
Standard
12S-HETE
A0A2L0ESU2
C
15S-HETE
Standard
15R-HETE
Standard
15R-HETE
S4XZS0
mAu
Time (min)

Fig. S5 Chiral-phase HPLC profiles of MonoHFAs obtained from the conversion of ARA (**1**) by the selected 3 putative LOXs derived from *S. cellulosum* (UniProtKB protein numbers, A0A2LESS6, A0A2L0ESU2, and S4XZS0) with 9*S*-, 9*R*-, 12*S*-, 12*R*-, 15*S*-, and 15*R*-HETE (**3**) standards. The MonoHFAs were analyzed using the Amylose-1 column. (A) Chiral-phase HPLC analysis of the product obtained from the conversion of **1** by the putative LOX cloned with the primer of A0A2LESS6 with 9*S*- and 9*R*-HETE standards. (B) Chiral-phase HPLC analysis of the product obtained from the conversion of **1** by LOX cloned with the primer of A0A2L0ESU2 with 12*S*- and 12*R*-HETE standards. (C) Chiral-phase HPLC analysis of the product obtained from the conversion of ARA by the putative LOX cloned with the primer of S4XZS0 with **3** and 15*S*-HETE standards. The reaction products of A0A2LESS6, A0A2L0ESU2, and S4XZS0 proteins were suggested as **3**, 12*S*-, and 9*S*-HETE, respectively.

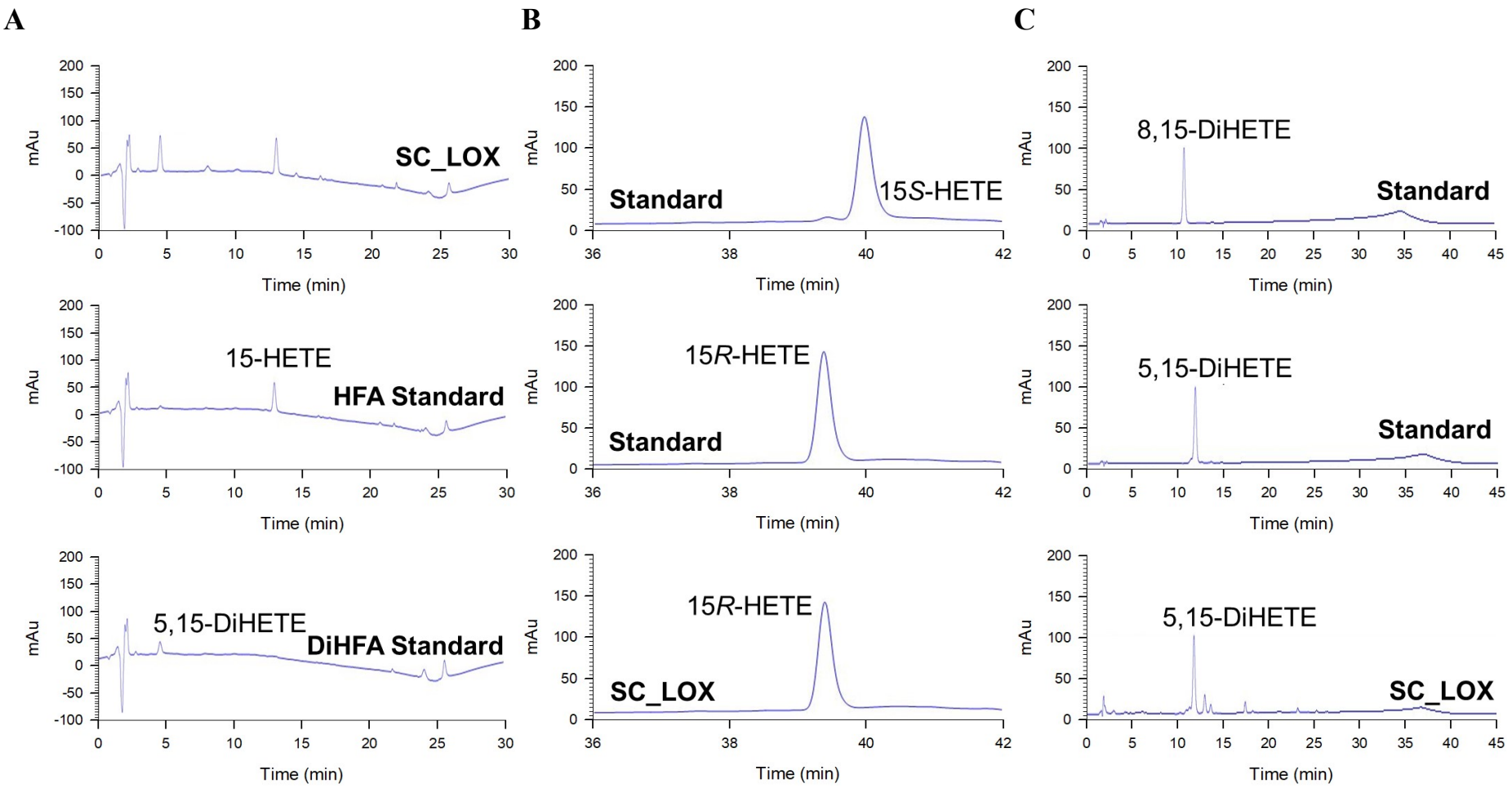

Fig. S6 Reverse- and chiral-phase HPLC profiles of the reaction products obtained from the conversion of ARA (**1**) by the putative LOX cloned with the primer of S4XZS0 with standards. (A) Reverse-phase HPLC profiles of the reaction products obtained from the conversion of **1** by the putative LOX with 15*S*-HETE (**3**) and 5*S*,15*S*-DiHETE (**4**) standards. The MonoHFAs were analyzed using the Nucleosil C18 column. (B) Chiral-

phase HPLC profiles of MonoHFA obtained from the biotransformation of **1** by the putative LOX with **3** and 15*S*-HETE standards. The MonoHFAs were analyzed using the Amylose-1 column. (C) Reverse-phase HPLC profiles of DiHFA obtained from the bioconversion of **1** by the putative LOX with 8*S*,15*S*-DiHETE and 5*S*,15*S*-DiHETE standards. The MonoHFAs were analyzed using the Nucleosil C18 column. The reactions were performed at 30 °C in 50 mM EPPS buffer (pH 8.0) containing 1.0 mM **1**, 0.1 g/L enzyme, and 100 mM cysteine as reducing agent for 10 min.

A

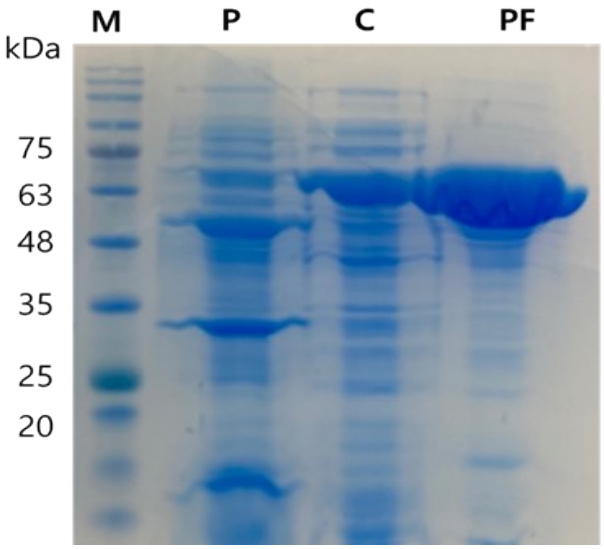

B

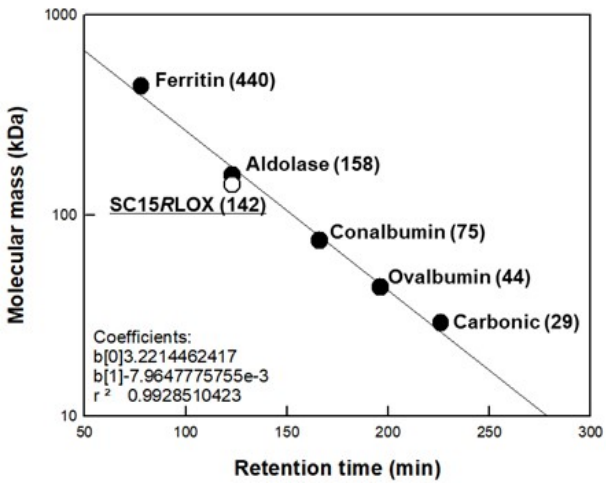

Fig. S7 SDS-PAGE analysis and gel filtration chromatography of *S. cellulosum* 15*R*-LOX expressed in *E. coli* C2566. (A) SDS-PAGE of *S. cellulosum* 15*R*-LOX. M, the protein marker; P, pellet; C, crude; PF, purified enzyme (*S. cellulosum* 15*R*-LOX). (B) Determination of the molecular mass of the purified native *S. cellulosum* 15*R*-LOX by using Sephacryl S-300 HR column with reference proteins. The reference proteins were carbonic (29 kDa), ovalbumin (44 kDa), conalbumin (75 kDa), aldolase (158 kDa), and ferritin (440 kDa).

A

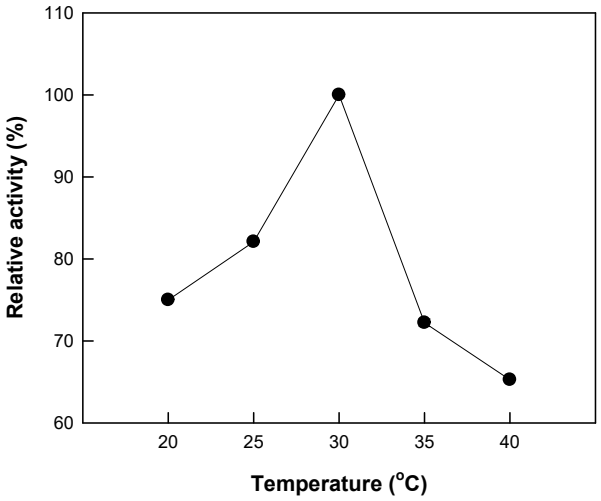

B

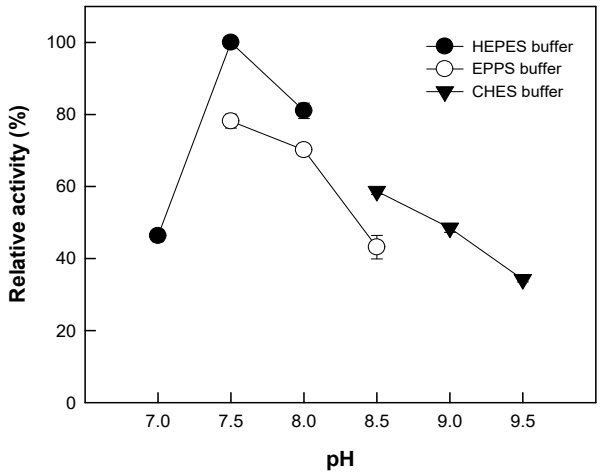

Fig. S8 Effects of temperature and pH on the production of 15*R*-HETE (**3**) from ARA (**1**) by 15*R*-LOX from *S. cellulosum*. (A) Effect of temperature on the biotransformation of ARA into 15*R*-HETE. The reactions were performed in 50 mM HEPES (pH 8.0) buffer containing 0.01 g/L enzyme and 0.5 mM ARA by varying the temperature from 20 to 40 °C in the presence of 100 mM cysteine for 10 min. (B) Effect of pH on the biotransformation of ARA into 15*R*-HETE. The reactions were performed using 50 mM HEPES, 50 mM EPPS, and 50 mM CHES buffers containing 0.01 g/L enzyme, 0.5 mM ARA, and 100 mM cysteine by varying the pH from 7.5 to 9.5 at 30 °C for 10 min. Data represent the mean ± SD (n = 3) values.

A

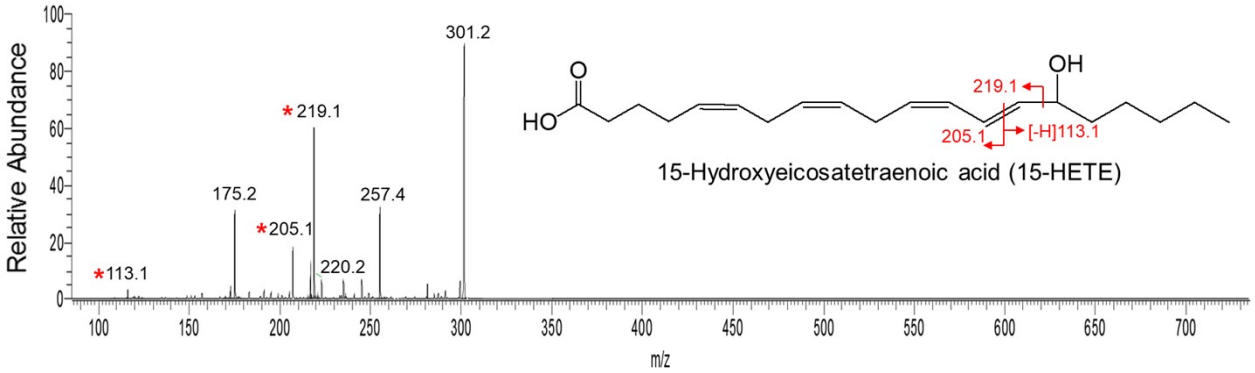

15-HETE

B

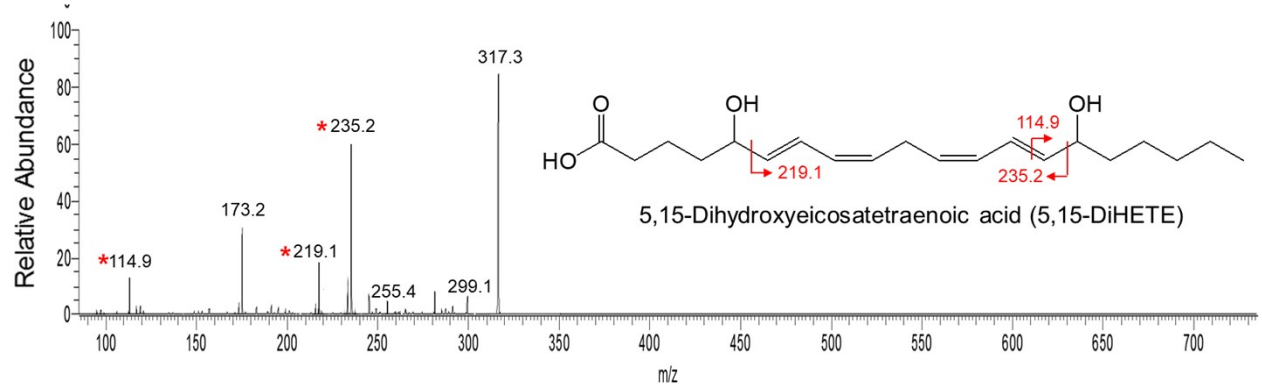

5,15-DiHETE

Fig. S9 LC-MS/MS profiles of MonoHFA and DiHFA obtained from the conversion of ARA (**1**) by 15*R*-LOX from *S. cellulosum*. The red arrows indicate critical fragments around the hydroxyl group. (A) 15-HETE. (B) 5,15-DiHETE.

A

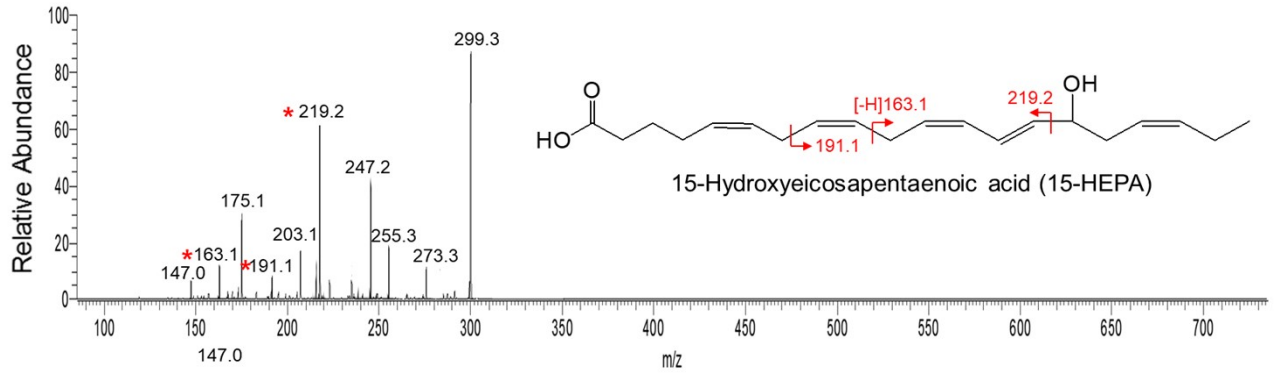

15-HEPA

B

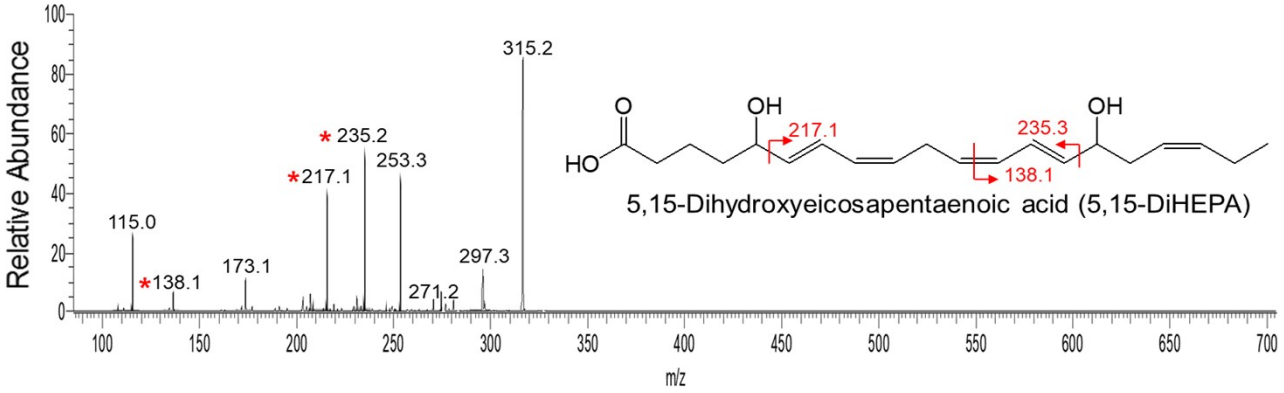

5,15-DiHEPA

Fig. S10 LC-MS/MS profiles of MonoHFA and DiHFA obtained from the conversion of EPA (**5**) by 15*R*-LOX from *S. cellulosum*. The red arrows indicate critical fragments around the hydroxyl group. (A) 15-HEPA. (B) 5,15-DiHEPA.

A

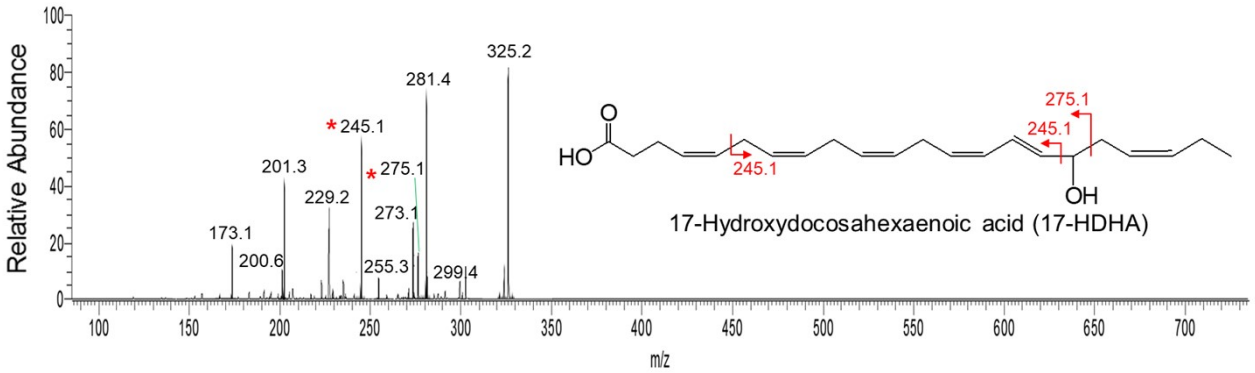

17-HDHA

B

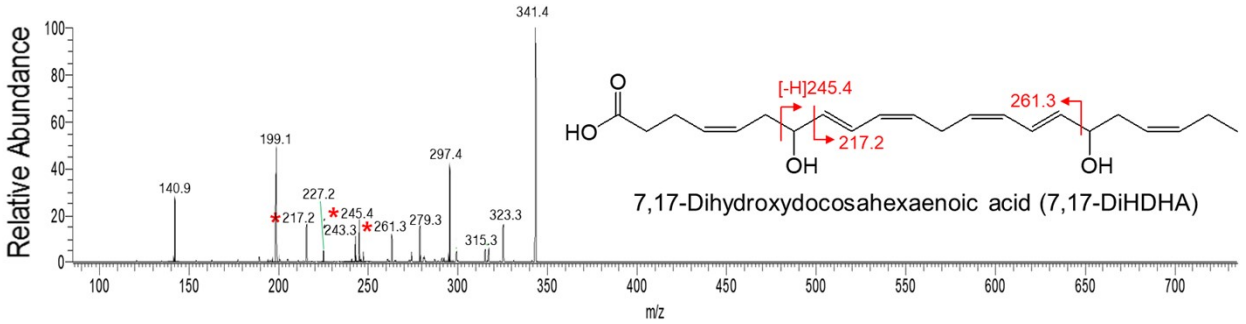

7,17-DiHDHA

Fig. S11 LC-MS/MS profiles of MonoHFA and DiHFA obtained from the conversion of DHA (**9**) by 15*R*-LOX from *S. cellulosum*. The red arrows indicate critical fragments around the hydroxyl group. (A) 17-HDHA. (B) 7,17-DiHDHA.

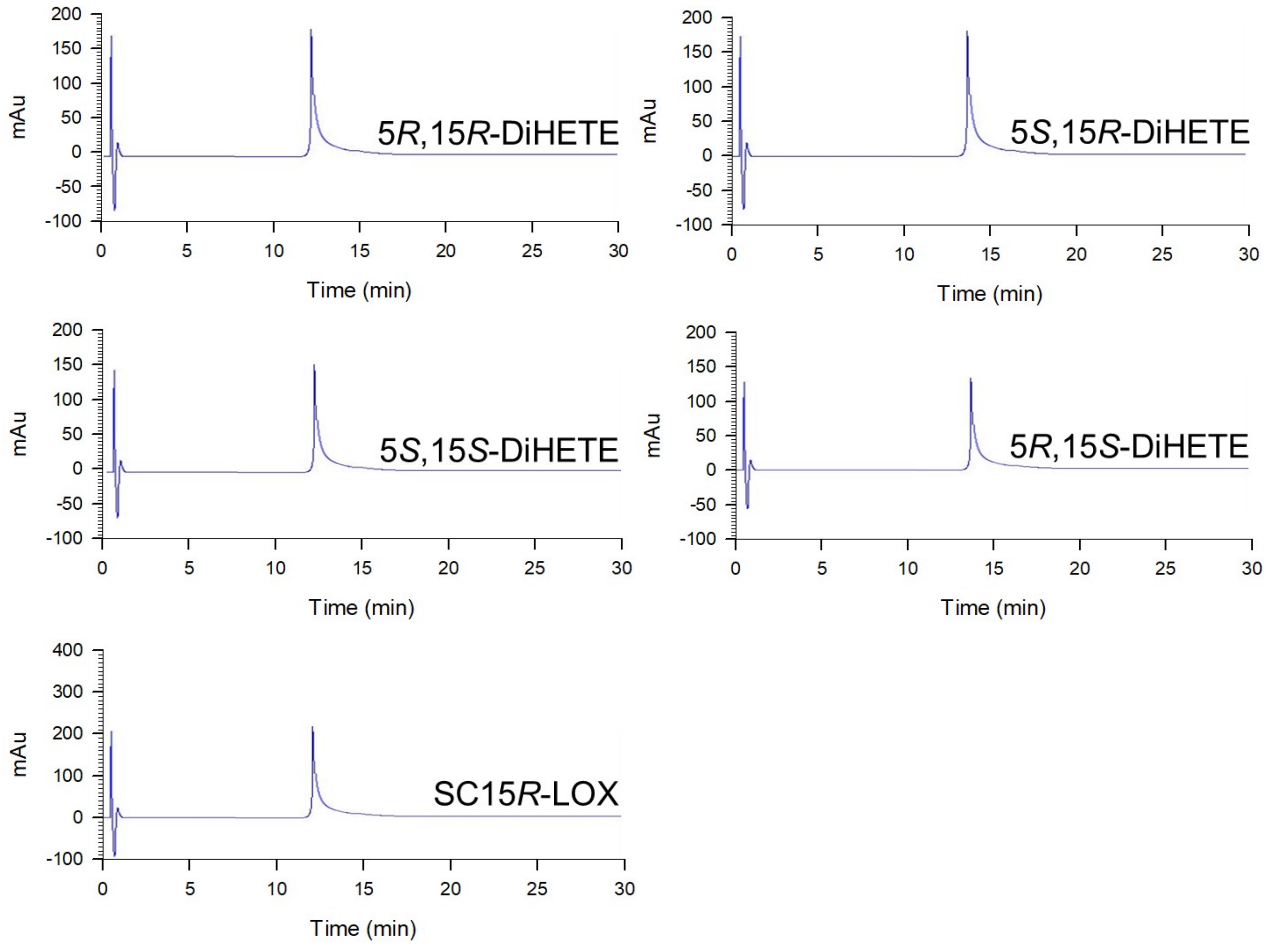

Fig. S12 Normal-phase HPLC profiles of DiHFA obtained from the conversion of ARA (**1**) by *S. cellulosum* 15*R*-LOX with 5*R*,15*S*-DiHETE, 5*S*,15*R*-DiHETE, 5*S*,15*S*-DiHETE, and 5*R*,15*R*-DiHETE (**4**) standards. The DiHFAs were analyzed using a Zorbax Rx-Sil column. The reactions were performed at 30 °C in 50 mM EPPS (pH 8.0) containing 1.0 mM **1**, 1.0 g/L enzyme, and 100 mM cysteine for 10 min. The compound is suggested as 5*R*,15*R*-DiHETE or 5*S*,15*S*-DiHETE. However, the chirality of the DiHFAs produced by double-oxygenating LOXs did not change from that of the MonoHFAs,[5-7] indicating that the product obtained from the conversion of 15*R*-HETE (**3**) by *S. cellulosum* 15*R*-LOX was **4**, but not 5*S*,15*S*-DiHETE. Furthermore, the NMR data for 5,15-DiHETE obtained from the conversion of **3** by *S. cellulosum* 15*R*-LOX were different from those of 5*S*,15*S*-DiHETE. The product obtained was thus 5*R*,15*R*-DiHETE.

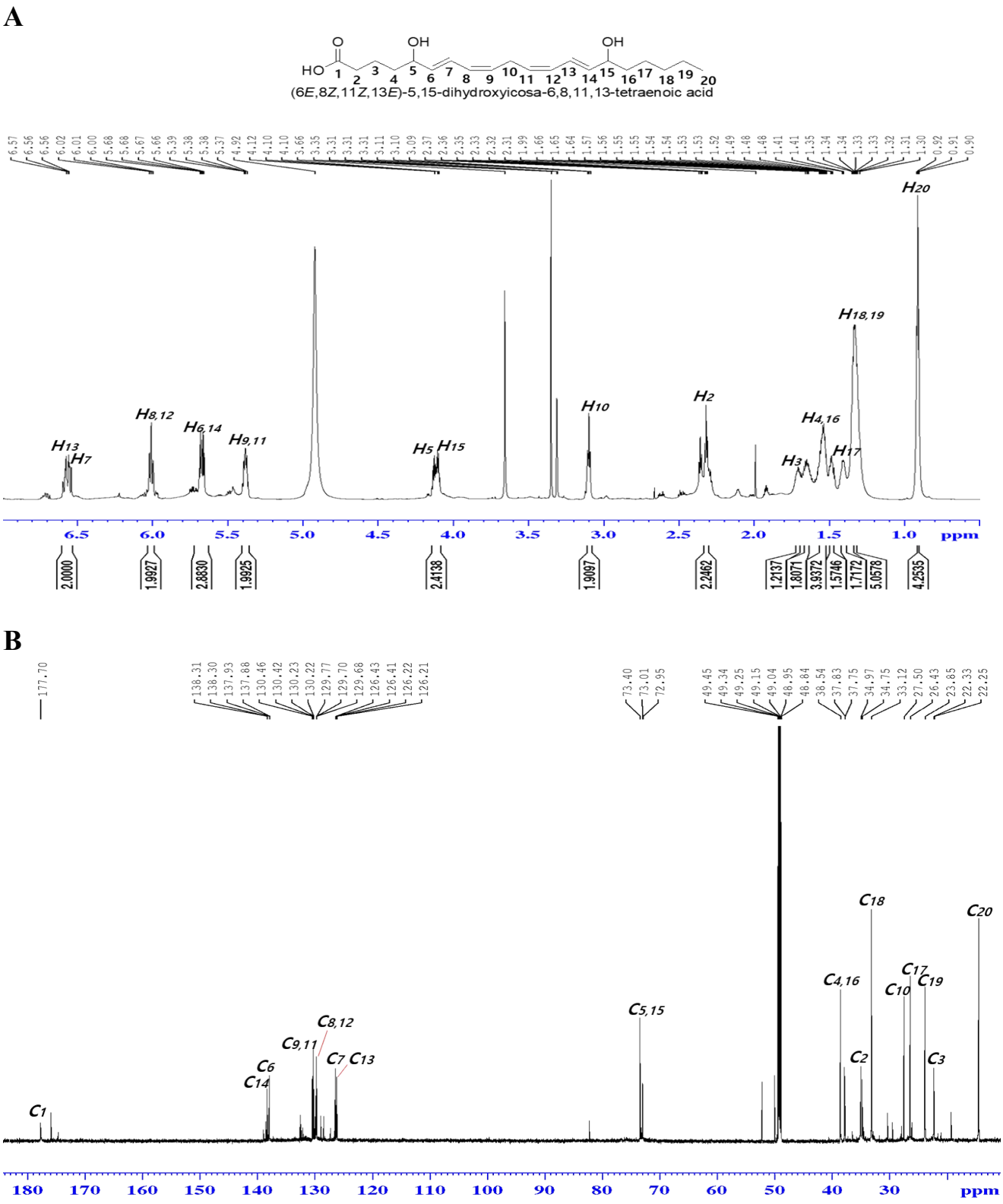

Fig. S13 ^{1}H NMR and ^{13}C NMR peaks of 5*R*,15*R*-DiHETE (isomer of leukotriene B4; **4**) in deuterated methanol (MeOD) (850 MHz NMR).

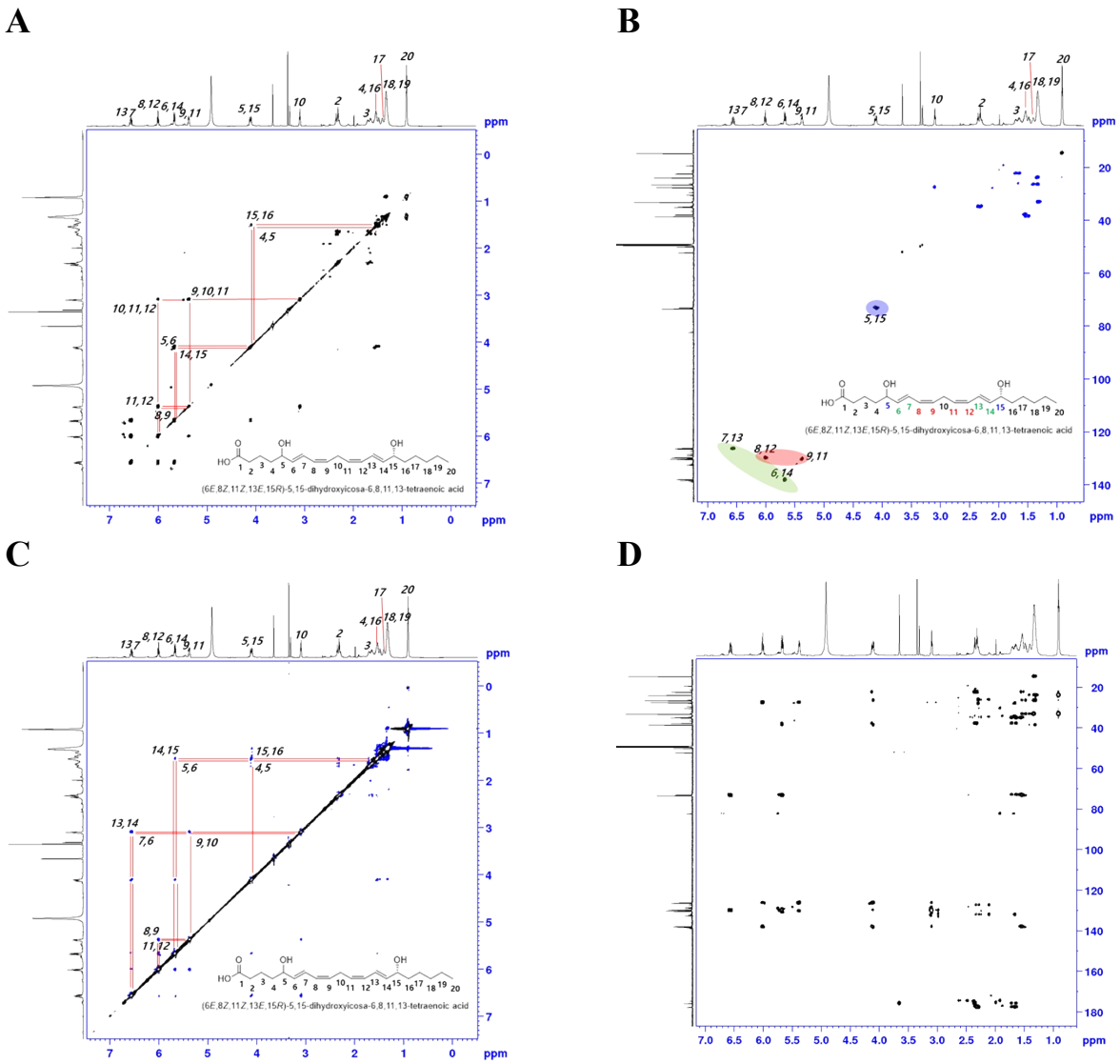

Fig. S14 2D NMR data of 5*R*,15*R*-DiHETE (**4**) in MeOD (850 MHz NMR). (A) Correlation spectroscopy (COSY). (B) Heteronuclear single quantum coherence (HSQC). (C) Rotating frame Overhauser enhancement spectroscopy (ROSEY). (D) Heteronuclear multiple bond coherence (HMBC).

A

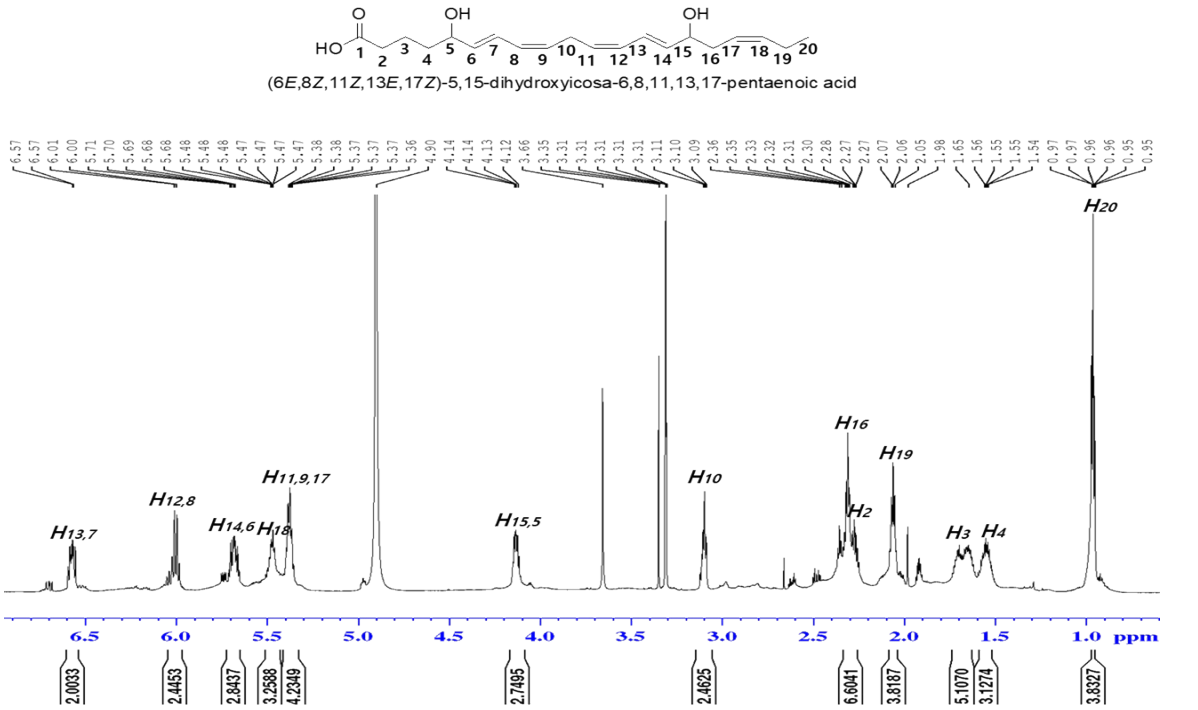

B

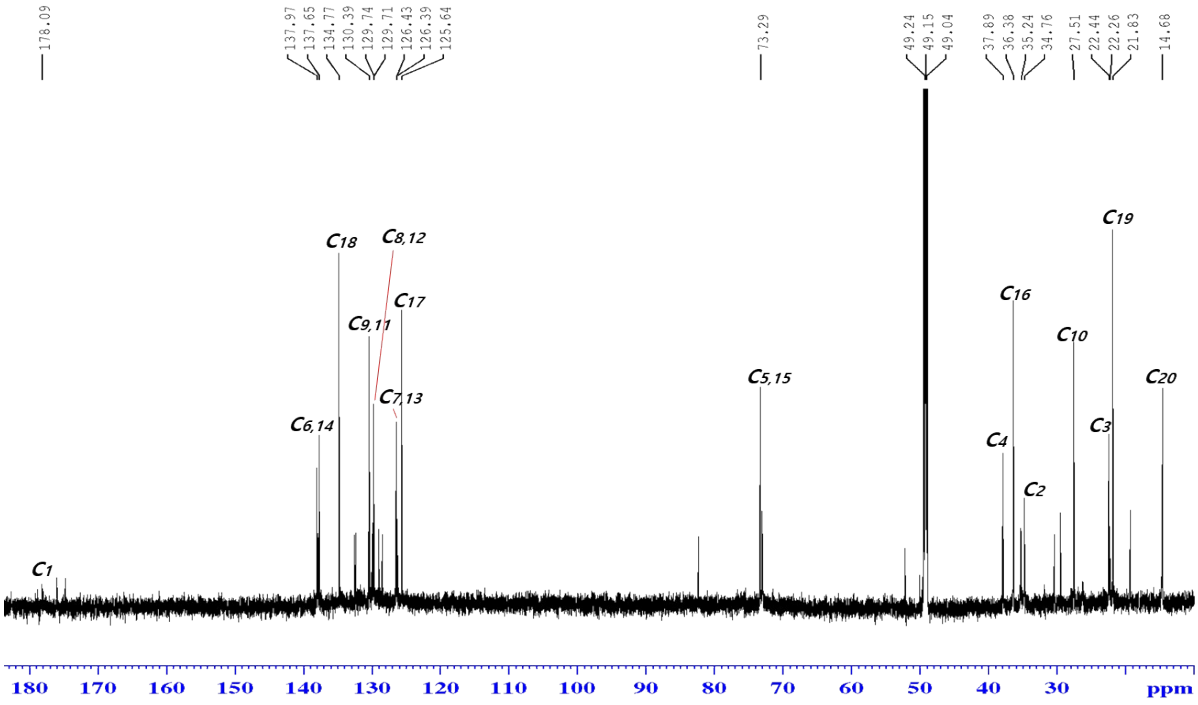

Fig. S15 ^{1}H NMR and ^{13}C NMR peaks of 5*R*,15*R*-DiHEPA (enantiomer of resolvin E4; **8**) in MeOD (850 MHz NMR).

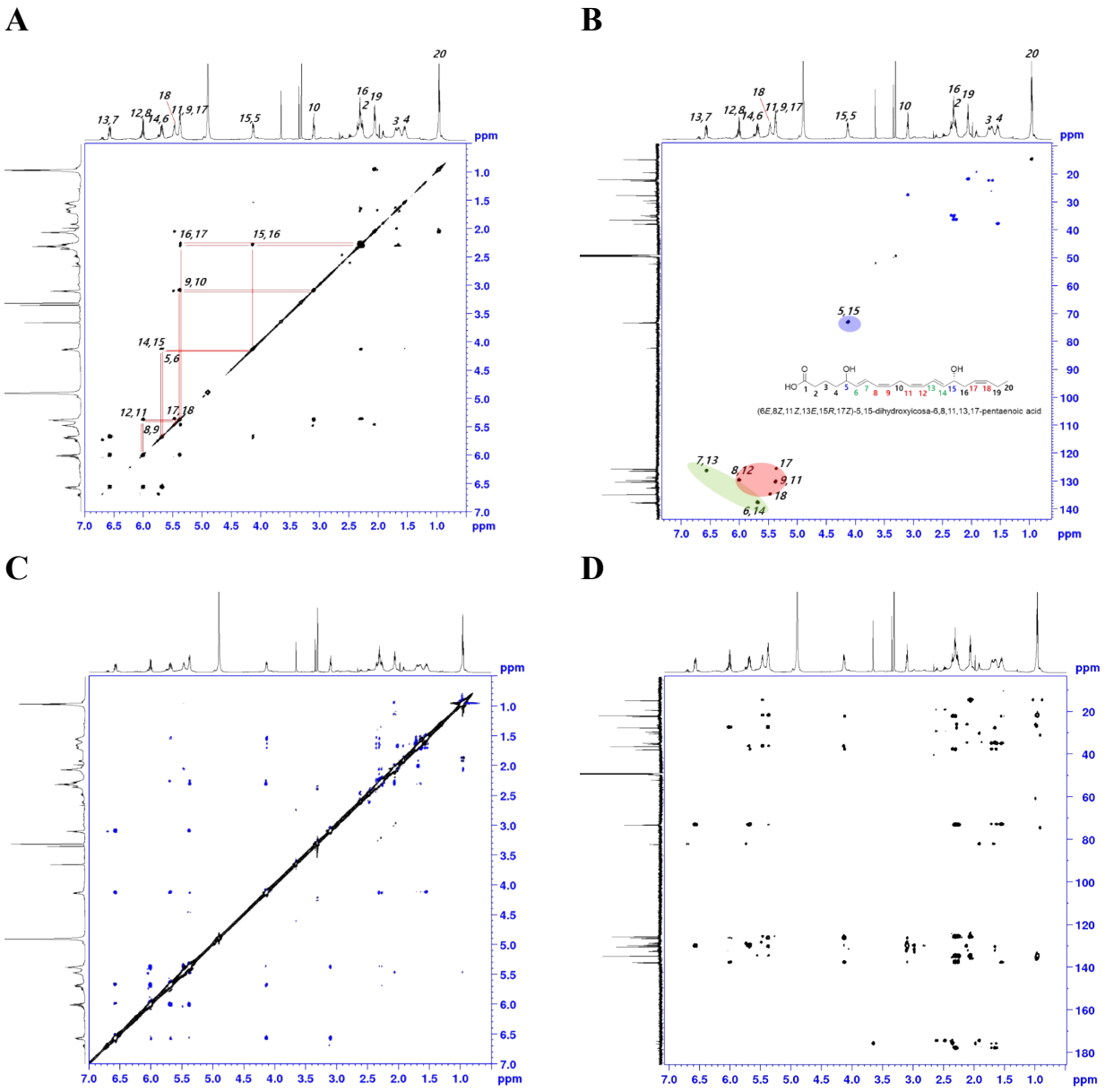

Fig. S16 2D NMR data of 5*R*,15*R*-DiHEPA (**8**) in MeOD (850 MHz NMR). (A) COSY. (B) HSQC. (C) ROSEY. (D) HMBC.

A

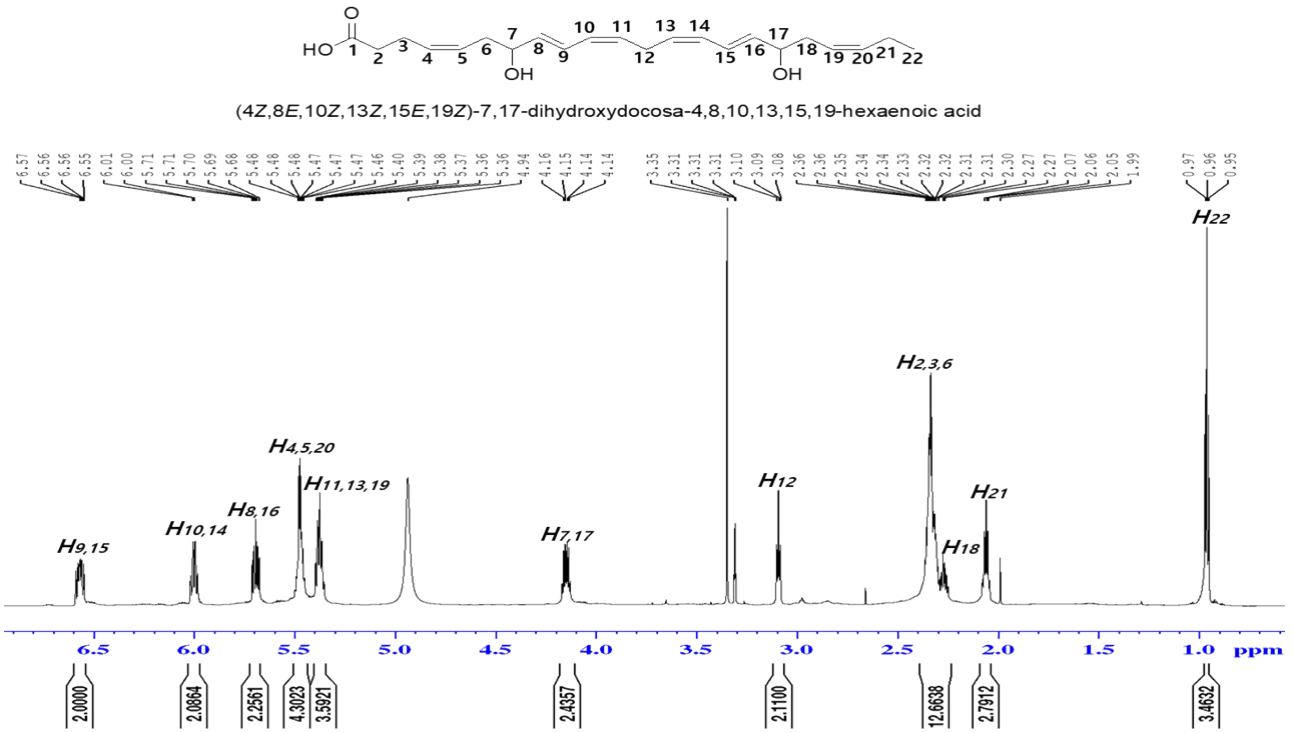

B

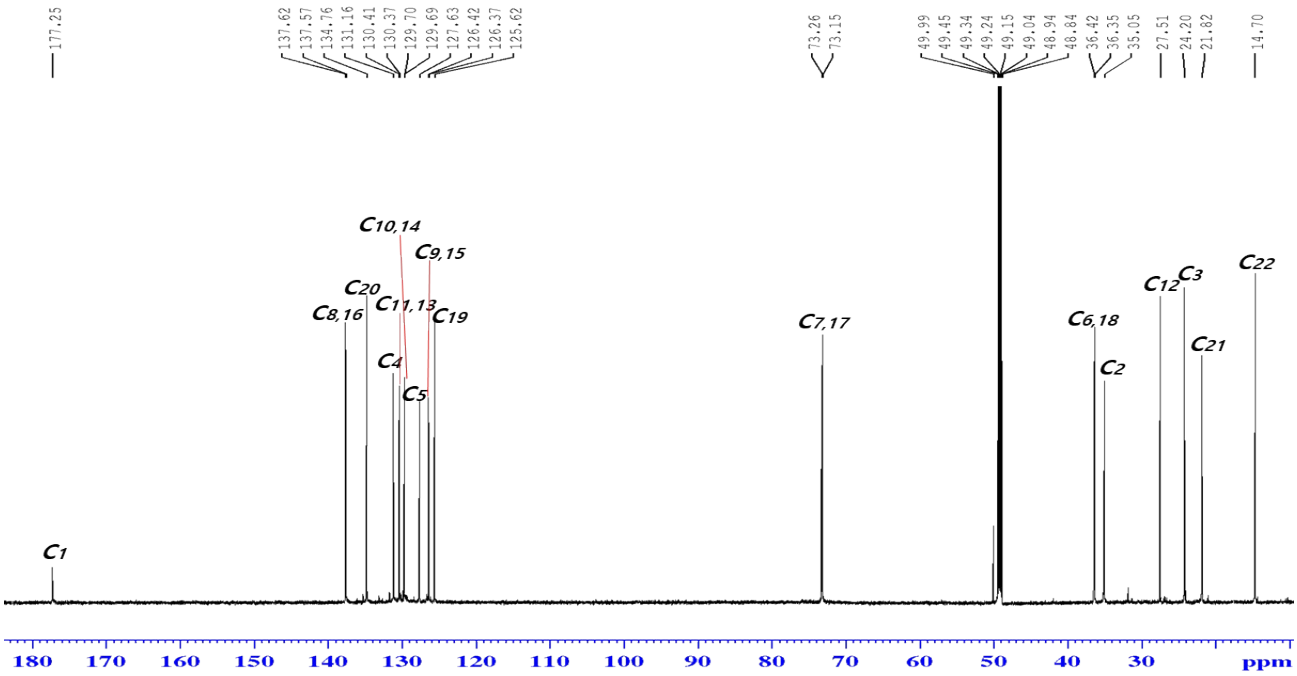

Fig. S17 ^{1}H NMR and ^{13}C NMR peaks of 7*R*,17*R*-DiHDHA (enantiomer of resolvin D5; **12**) in MeOD (850 MHz NMR).

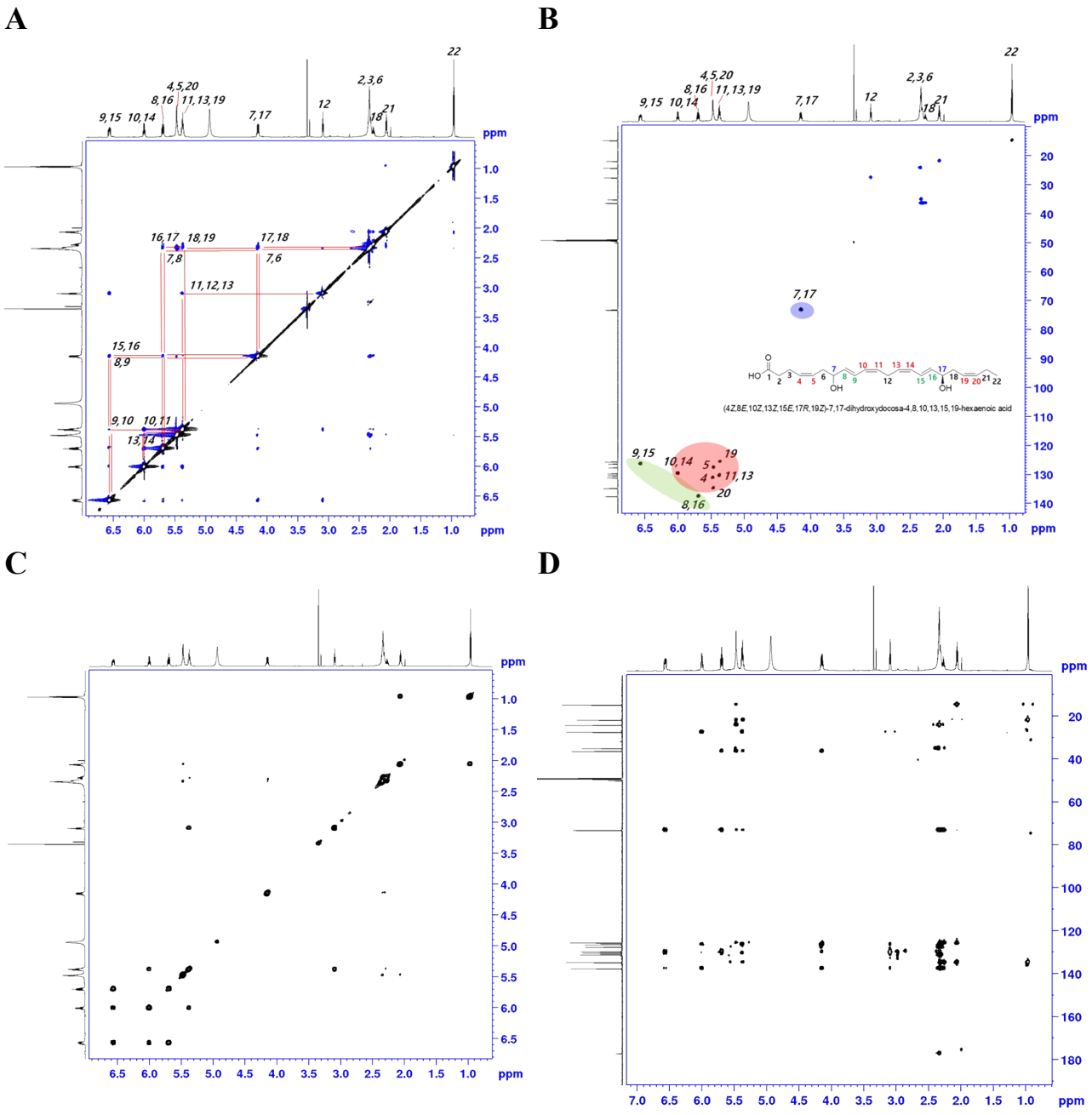

Fig. S18 2D NMR data of 7*R*,17*R*-DiHDHA (**12**) in MeOD (850 MHz NMR). (A) COSY. (B) HSQC. (C) ROSEY. (D) HMBC.

A

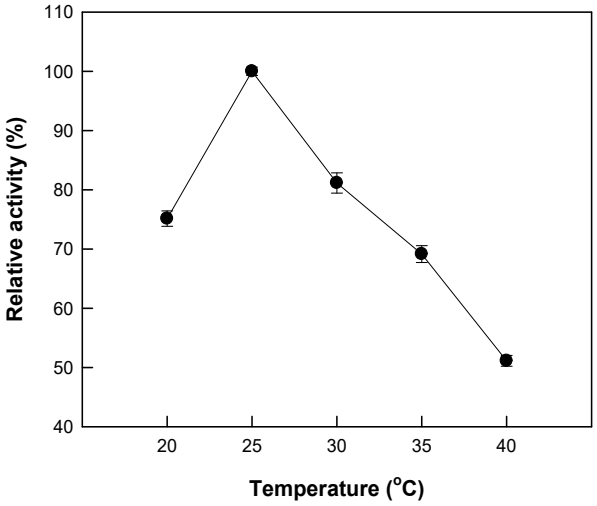

B

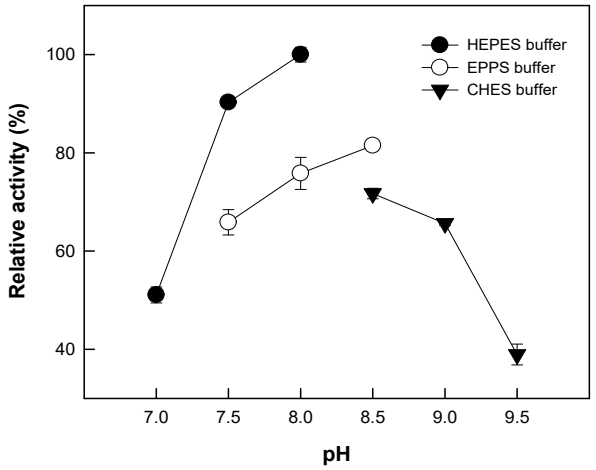

Fig. S19 Effects of temperature and pH on the biotransformation of ARA (**1**) into 5*R*,15*R*-DiHETE (**4**) by *E. coli* expressing 15*R*-LOX from *S. cellulosum*. (A) Effect of temperature on the biotransformation of **1** into **4**. The reactions were performed in 50 mM HEPES (pH 8.0) buffer containing 1.0 g/L cells, 1.0 mM **1**, and 100 mM cysteine by varying the temperature from 20 to 40 °C with 100 mM cysteine for 60 min. (B) Effect of pH on the biotransformation of **1** into **4**. The reactions were performed in 50 mM HEPES, 50 mM EPPS, and 50 mM CHES buffers by varying the pH from 7.5 to 9.5 containing 1.0 g/L cells, 1.0 mM **1**, and 100 mM cysteine at 25 °C for 60 min. Data represent the mean ± SD (n = 3) values.

A

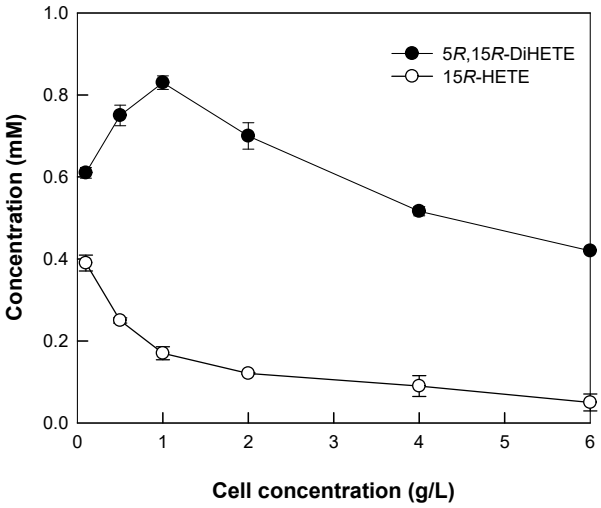

B

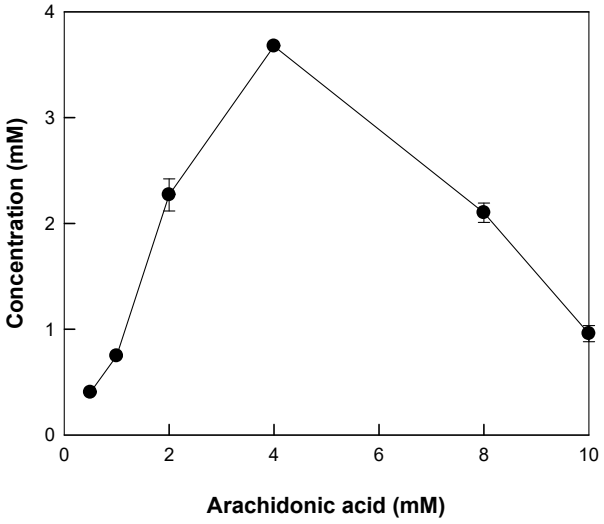

Fig. S20 Optimization of cell and substrate concentrations for the biotransformation of ARA (**1**) into 5*R*,15*R*-DiHETE (**4**) by *E. coli* expressing 15*R*-LOX from *S. cellulosum*. (A) Optimization of cell concentration. The reactions were performed in HEPES (pH 8.0) buffer containing 1.0 mM **1** and 100 mM cysteine by varying the cell concentration from 0.1 to 6.0 g/L cells for 60 min. (B) Optimization of substrate concentration. The reactions were performed in HEPES (pH 8.0) buffer containing 1.0 g/L cells and 100 mM cysteine by varying the concentration of **1** as substrate from 0.5 to 10 mM for 60 min. Data represent the mean ± SD (n = 3) values.

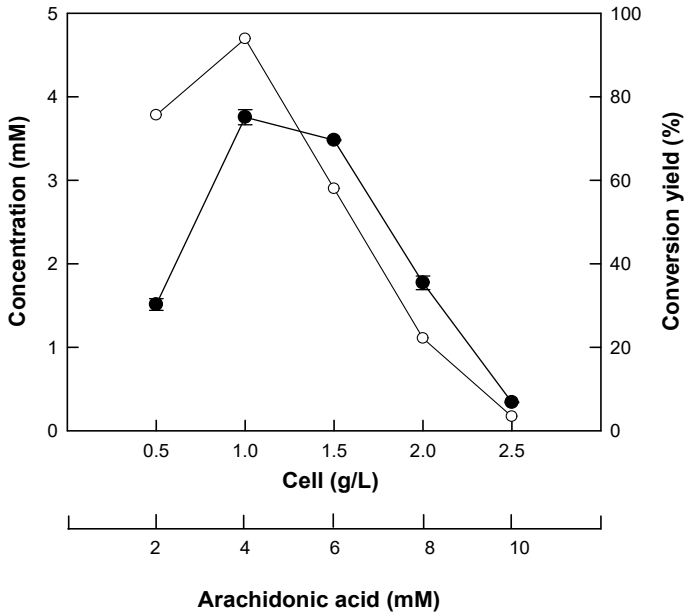

Fig. S21 Optimization of cell and substrate concentrations for the biotransformation of ARA (**1**) into 5*R*,15*R*-DiHETE (**4**) by *E. coli* expressing 15*R*-LOX from *S. cellulosum* at the optimal ratio of cells to substrate. The reactions were performed in a 100-mL flask containing 10 mL HEPES (pH 8.0) buffer supplemented with resin SP825 at the optimal ratio of 5:4 (g/L per mM) by varying the concentrations of cells and **1** from 0.5 g/L and 2.0 mM to 2.5 g/L and 10.0 mM at the optimal ratio of 1.0 g/L to 4.0 mM for 60 min. The symbols indicate the concentration (●) and conversion yield (%) (○) of **4**. Data represent the mean ± SD (n = 3) values.

A

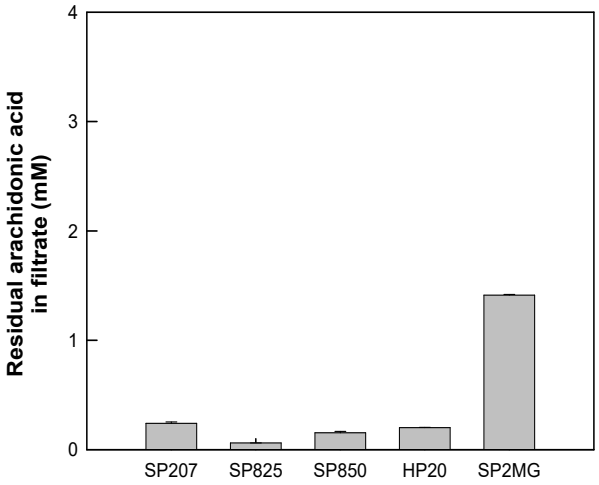

B

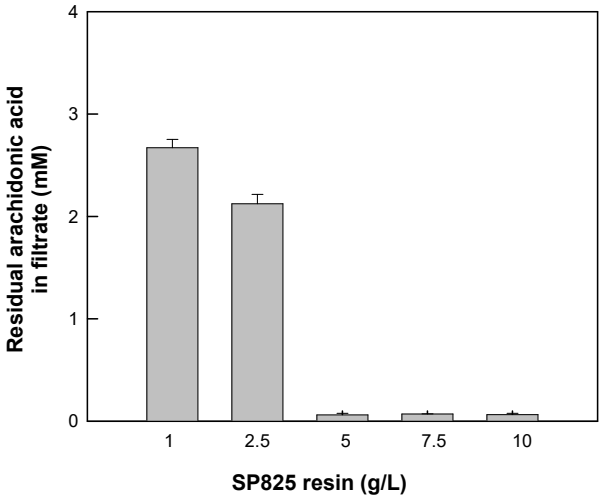

Fig. S22 Binding of absorbent resins to ARA (**1**) as a substrate. (A) Selection of absorbent resins for **1** as substrate. Adsorbent resins were used to test binding to **1**. (B) Effect of SP825 resin concentration on **1** at 4.0 mM. The reaction was performed in a 100-mL flask containing 10 mL 50 mM HEPES (pH 8.0) buffer supplemented 4.0 mM **1**, 1.0 g/L cells, and 100 mM cysteine with 5.0 g/L resin at 25 °C for 60 min. The resin and buffer were separated by filtration through a 45-μm pore-size filter. Data represent the mean ± SD (n = 3) values.

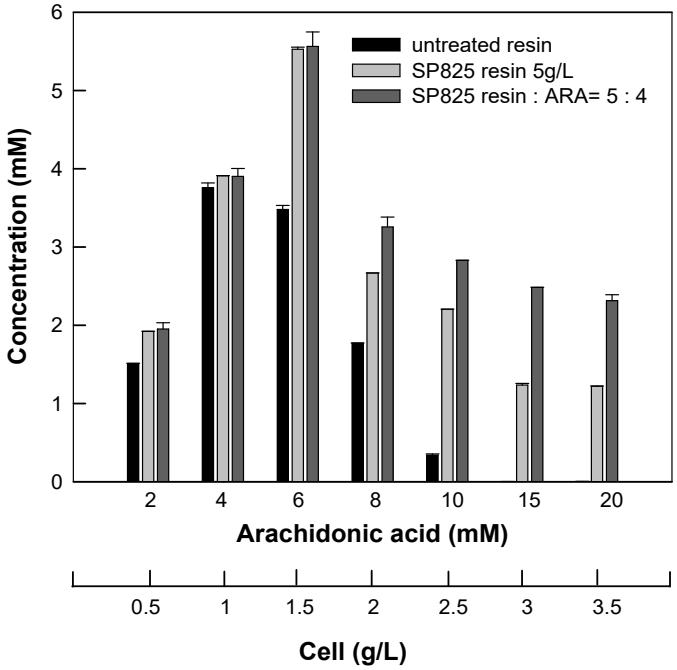

Fig. S23 Effect of resin SP825 concentration on the biotransformation of ARA (**1**) into 5*R*,15*R*-DiHETE (**4**) by 15*R*-LOX from *S. cellulosum* with varying the concentrations of cells and ARA (**1**). The reactions were performed at 25 °C in a 100-mL flask containing 10 mL reaction HEPES buffer (pH 8.0) with 100 mM cysteine by varying the concentrations of cells and **1** from 0.5 g/L and 2.0 mM to 3.5 g/L and 20 mM for 60 min. Dark, grey, and dark grey bars indicate the concentrations of **4** after the reactions without resin, with the optimal ratio of cells to substrate (1:4, g/L per mM) at a constant concentration of 5.0 g/L resin, and with the optimal ratio of cells, substrate, and resin resin (1:4:5, g/L per mM per g/L), respectively. Data represent the mean ± SD (n = 3) values.

A

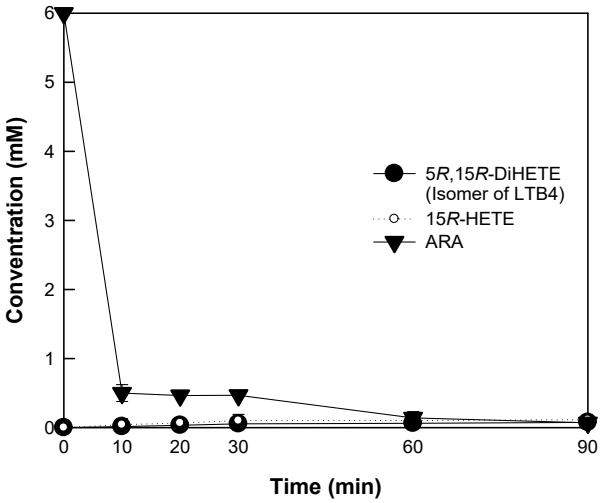
Conventration (mM)
Time (min)
5R,15R-DiHETE
(Isomer of LTB4)
15R-HETE
ARA

B

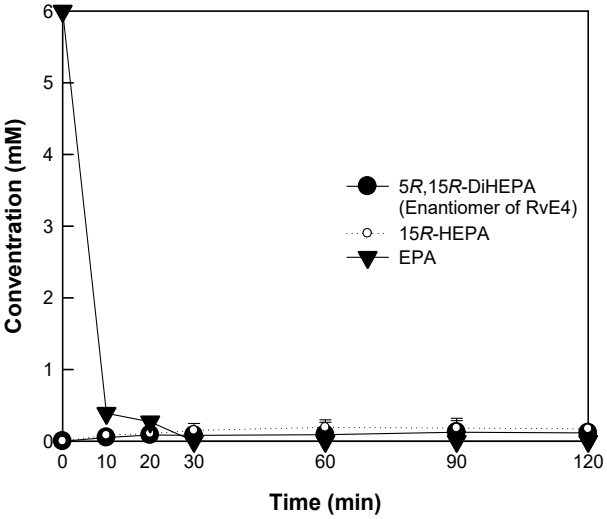
Conventration (mM)
Time (min)
5R,15R-DiHEPA
(Enantiomer of RvE4)
15R-HEPA
EPA

C

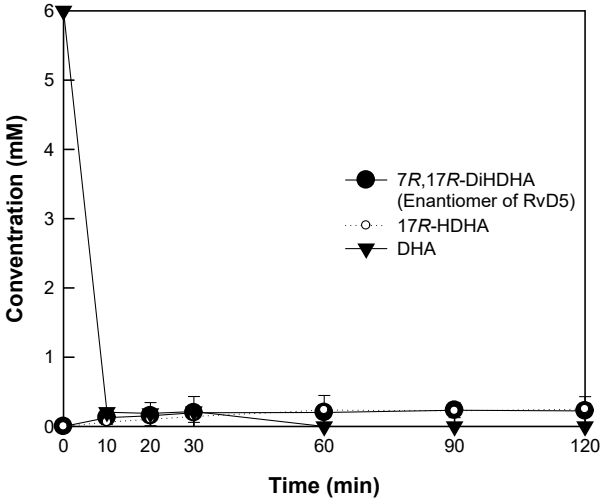
Conventration (mM)
Time (min)
7R,17R-DiHDHA
(Enantiomer of RvD5)
17R-HDHA
DHA

Fig. S24 Biotransformation of PUFAs into DiHFAs with the addition of resin by *E. coli* expressing 15*R*-LOX from *S. cellulosum* in filtrate. (A) Biotransformation of ARA (**1**) to 5*R*,15*R*-DiHETE (isomer of LTB4; **4**). (B) Biotransformation of EPA (**5**) to 5*R*,15*R*-DiHEPA (enantiomer of RvE4; **8**). (C) Biotransformation of DHA (**9**) to 7*R*,17*R*-DiHDHA (enantiomer of RvD5; **12**). The reactions were performed at 25 °C in a 100-mL flask containing 50 mM HEPES (pH 8.0) buffer supplemented with 7.5 g/L absorbent resin SP825, 6.0 mM PUFAs, 1.5 g/L cells, and 100 mM cysteine for 90 and 120 min. The resin and buffer were separated by filtration through a 45-μm pore-size filter. Data represent the mean ± SD (n = 3) values.

A

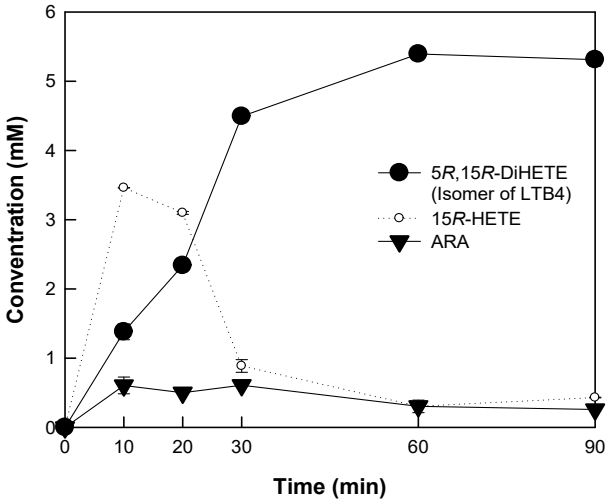
Conventration (mM)
Time (min)
5R,15R-DiHETE
(Isomer of LTB4)
15R-HETE
ARA

B

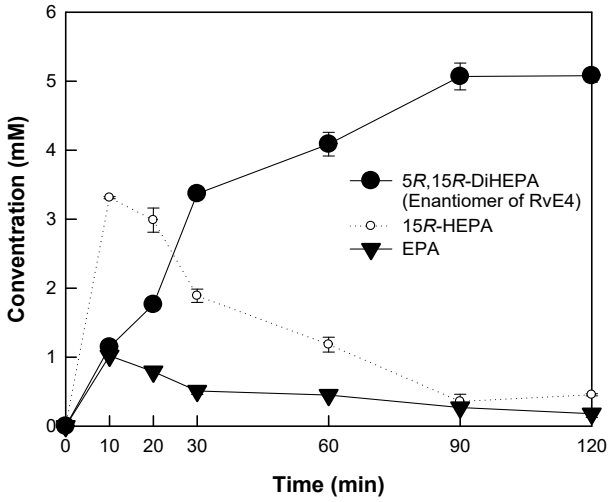
Conventration (mM)
Time (min)
5R,15R-DiHEPA
(Enantiomer of RvE4)
15R-HEPA
EPA

C

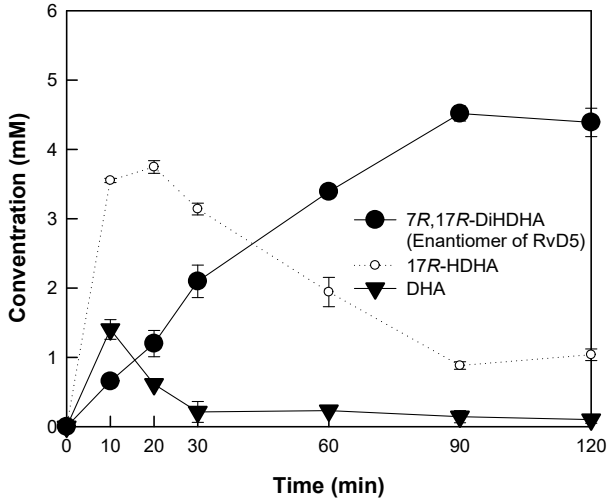
Conventration (mM)
Time (min)
7R,17R-DiHDHA
(Enantiomer of RvD5)
17R-HDHA
DHA

Fig. S25 Biotransformation of PUFAs into DiHFAs with the addition of resin by *E. coli* expressing 15*R*-LOX from *S. cellulosum* in resin. (A) Biotransformation of ARA (**1**) into 5*R*,15*R*-DiHETE (isomer of LTB4; **4**). (B) Biotransformation of EPA (**5**) into 5*R*,15*R*-DiHEPA (enantiomer of RvE4; **8**). (C) Biotransformation of DHA (**9**) into 7*R*,17*R*-DiHDHA (enantiomer of RvD5; **12**). The reactions were performed at 25 °C in a 100-mL flask containing 50 mM HEPES (pH 8.0) buffer supplemented with 7.5 g/L absorbent resin SP825, 6.0 mM PUFA, 1.5 g/L cells, and 100 mM cysteine for 90 and 120 min. The resin and buffer were separated by filtration through a 45-μm pore-size filter. Data represent the mean ± SD (n = 3) values.

A

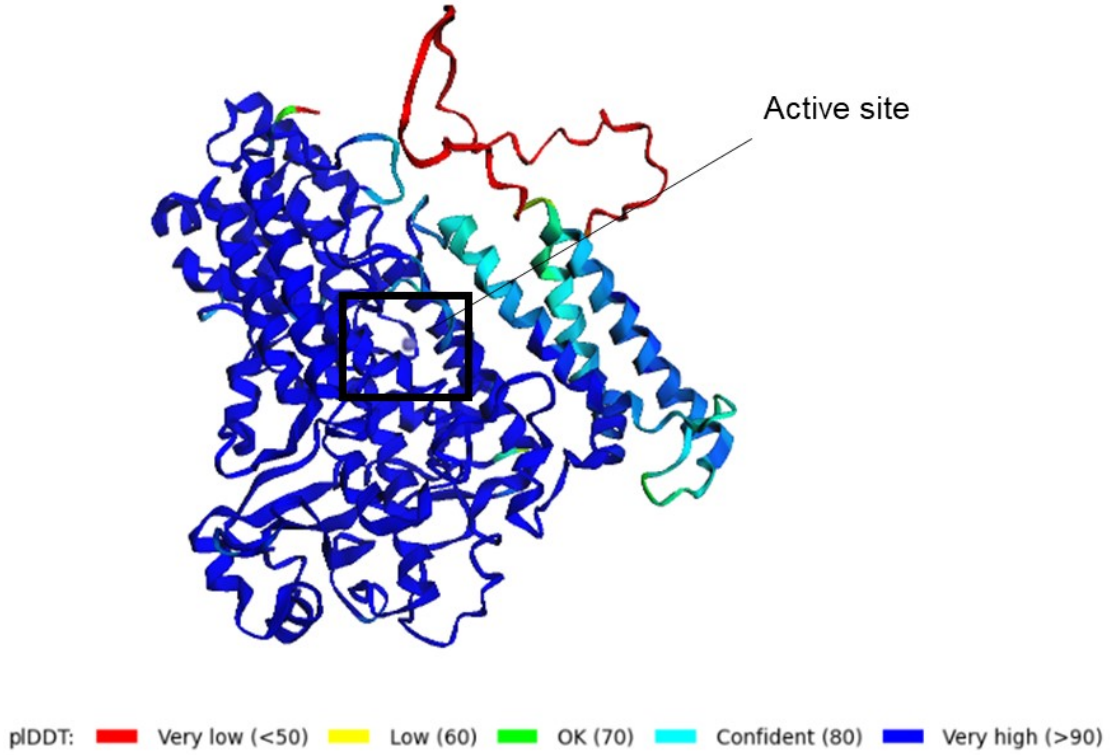
Active site
plDDT:
Very low (<50)
Low (60)
OK (70)
Confident (80)
Very high (>90)

B

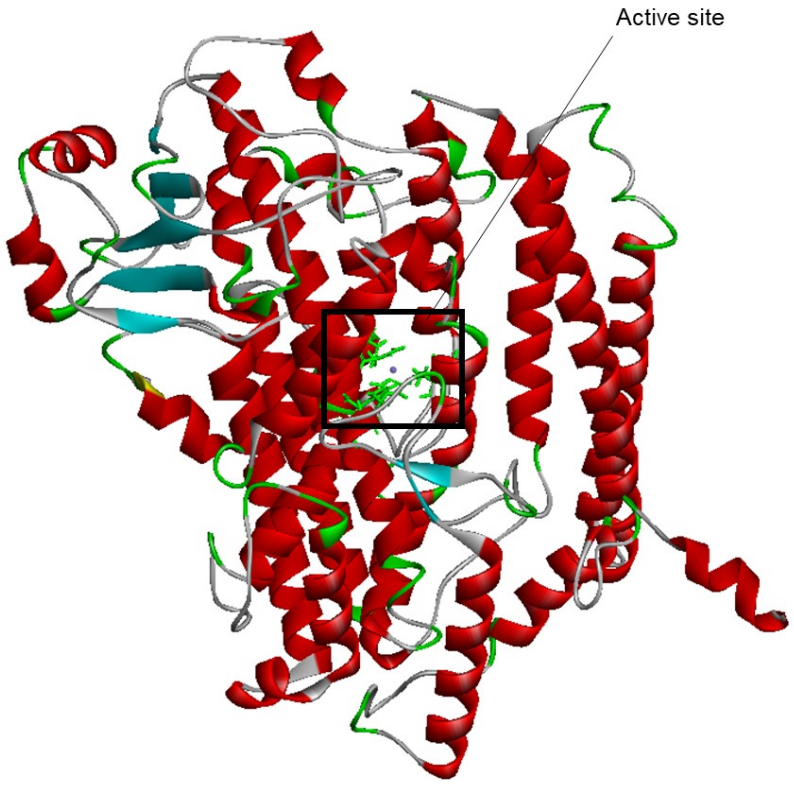
Active site

C

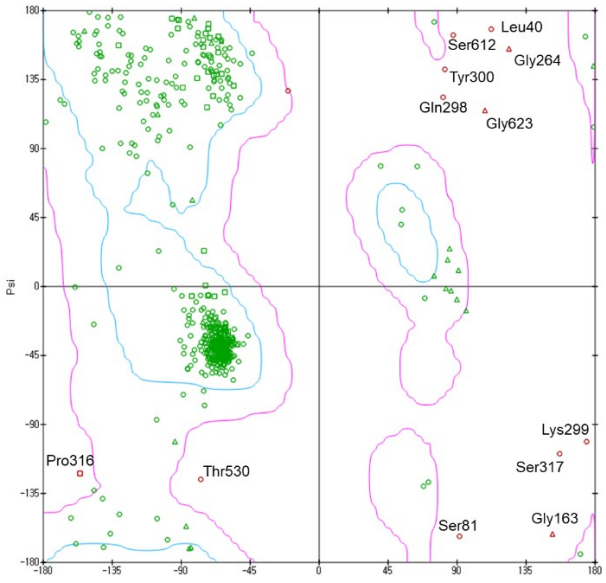

Fig. S26 Reliability of the models of 15*R*-LOX from *S. cellulosum* built by Alphafold and Discovery studio (DS). (A) Alphafold model. Blue color represents high reliability, whereas the remaining colors represent low reliability. (B) DS model. (C) Ramachandran plot for demonstrating reliability in DS model. The Ramachandran plot was shown with the verify score, and the residues displayed represents low reliability.

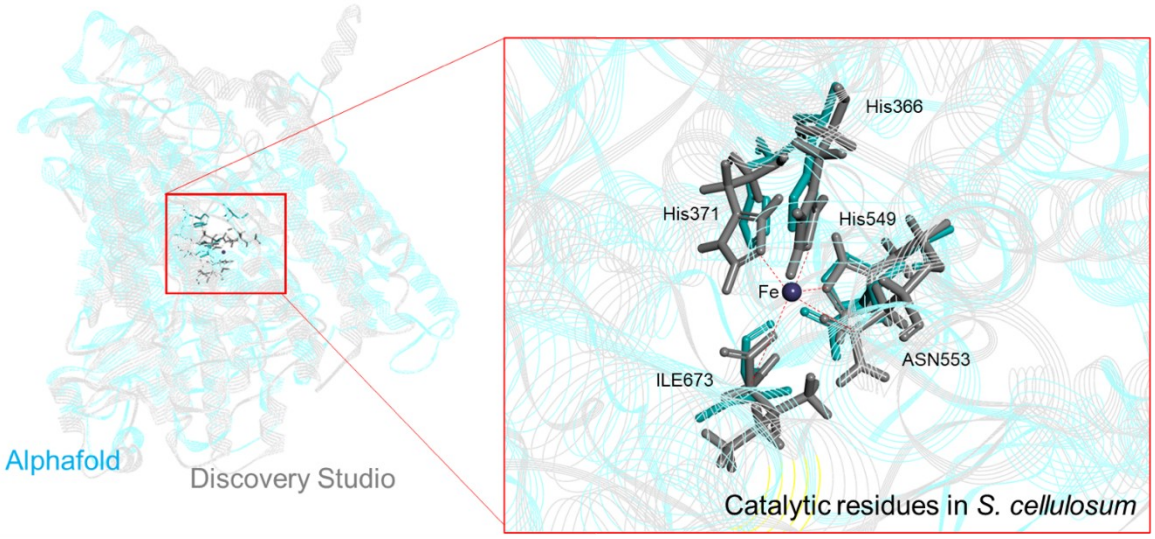

Fig. S27 Confirmation of the active site in 15*R*-LOX from *S. cellulosum* in DS model by Alphafold model. Superimposition of the catalytic residues built by Alphafold and DS. The catalytic residues His366/His371/His549/Asn553/Ile673 in the model built by Alphafold is shown in cyan whereas the those in the model built by DS is shown in gray. When the substrates were docked, interaction residues (Gln354, Leu413, Val602, Met603, and Leu606) are located at the hydrophobicity region of the substrate-binding pocket.

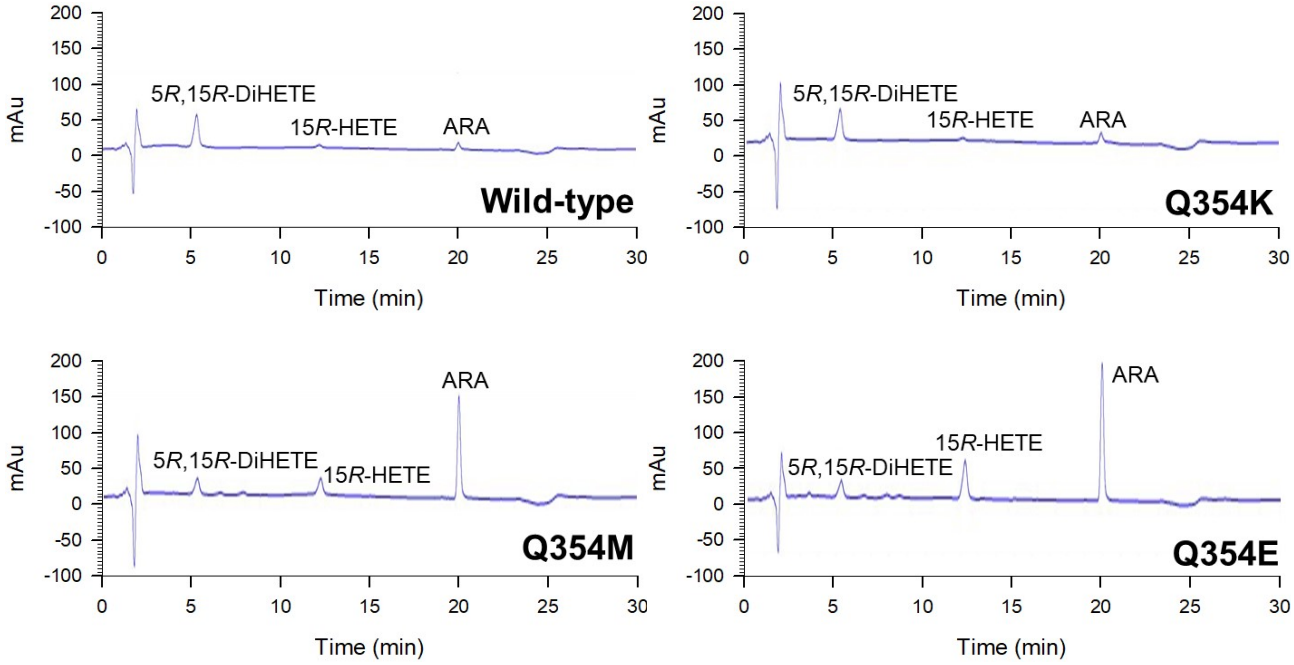

Fig. S28 Reverse-phase HPLC profiles of the products obtained from the conversion of ARA (**1**) by the wild-type and variant LOXs at position 354 from *S. cellulosum*. The MonoHFAs and DiHFAs were analyzed using the Nucleosil C18 column. The reactions were performed at 25 °C in 50 mM HEPES (pH 8.0) containing 1.0 mM **1**, 0.5 g/L cells, and 100 mM cysteine for 120 min.

A

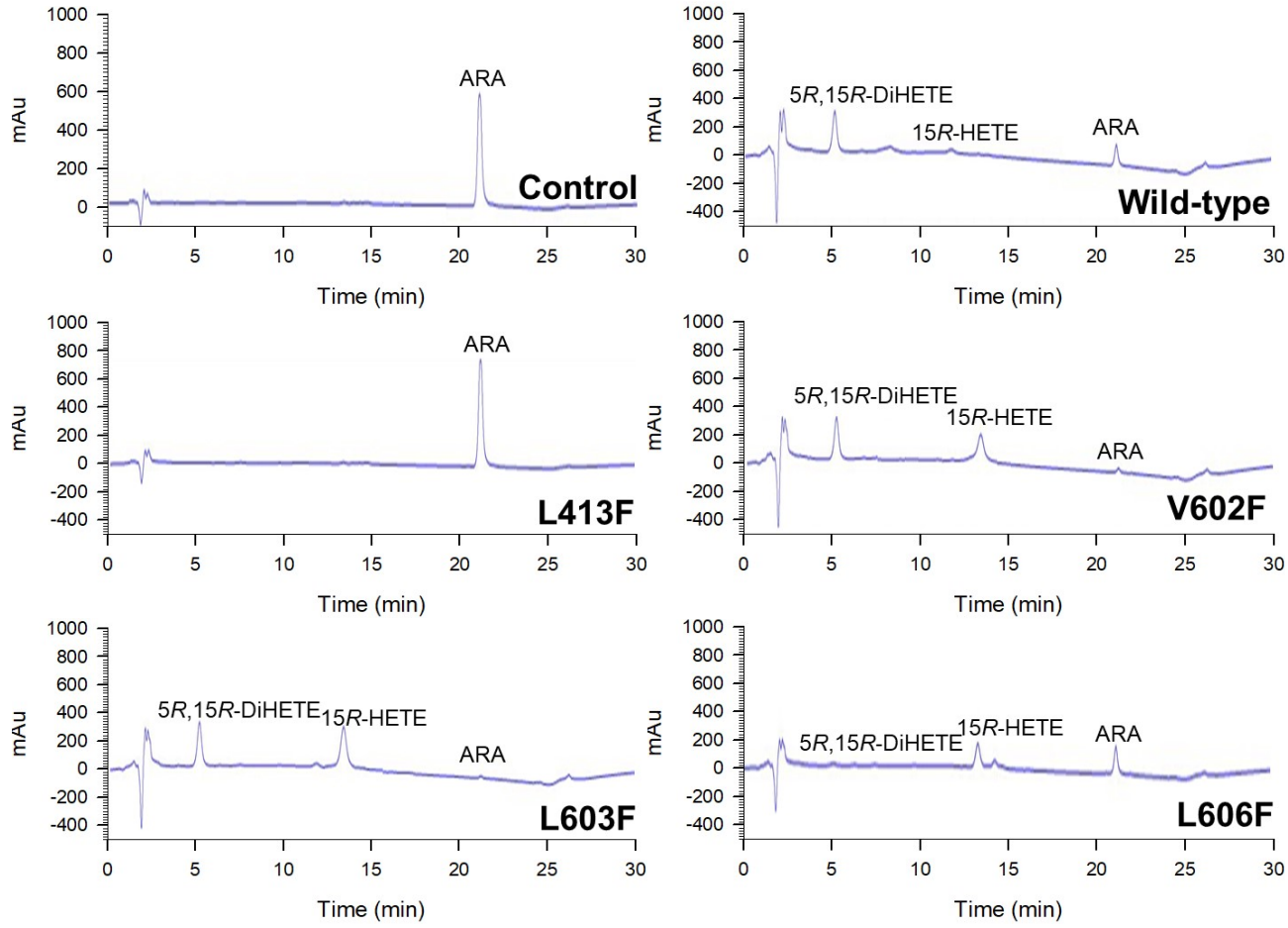
mAu
Time (min)
ARA
Control
5R,15R-DiHETE
15R-HETE
ARA
Wild-type
ARA
L413F
5R,15R-DiHETE
15R-HETE
ARA
V602F
5R,15R-DiHETE
15R-HETE
ARA
L603F
5R,15R-DiHETE
15R-HETE
ARA
L606F

B

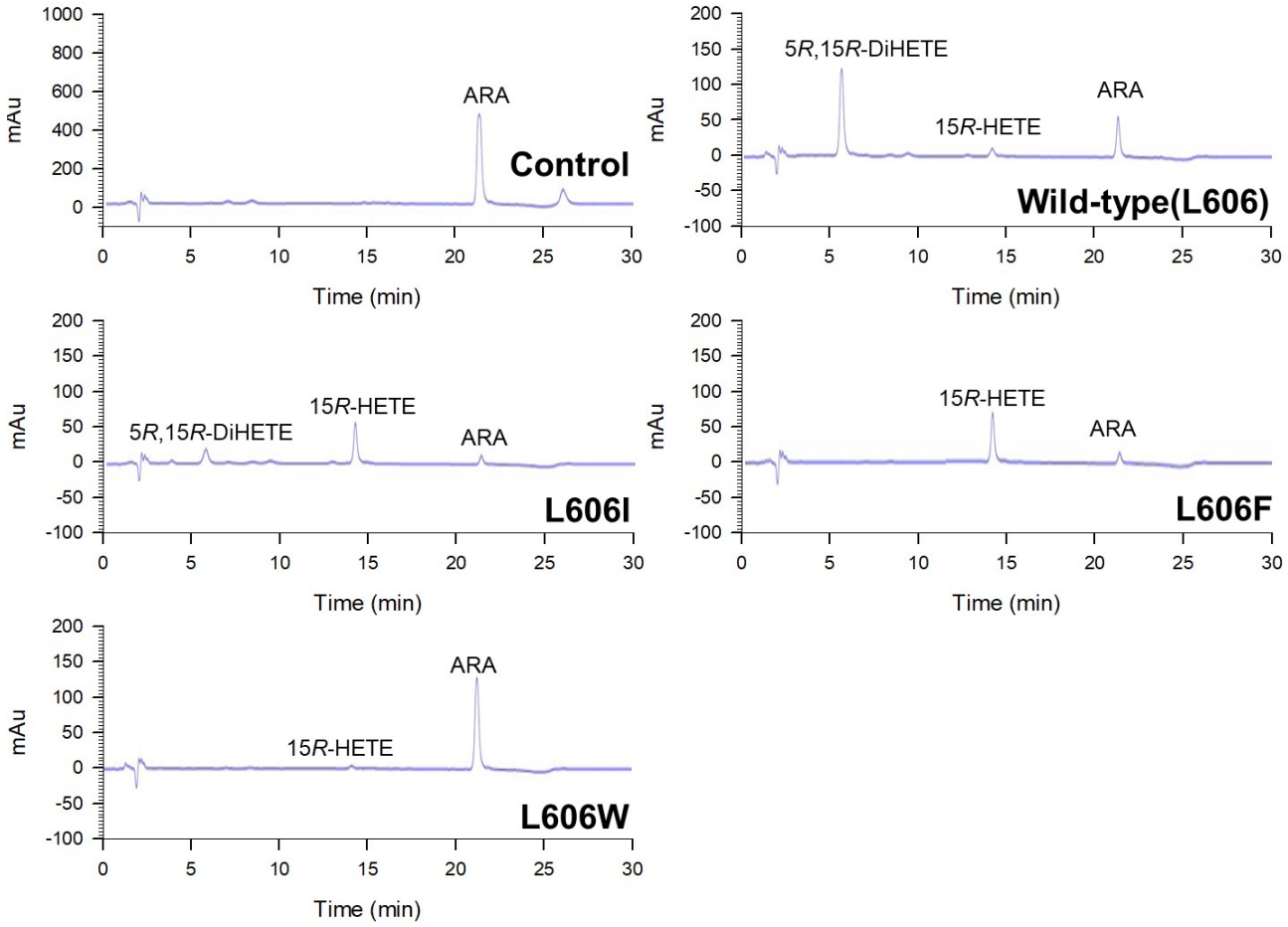
mAu
Time (min)
ARA
Control
5R,15R-DiHETE
15R-HETE
Wild-type(L606)
L606I
L606F
L606W

C

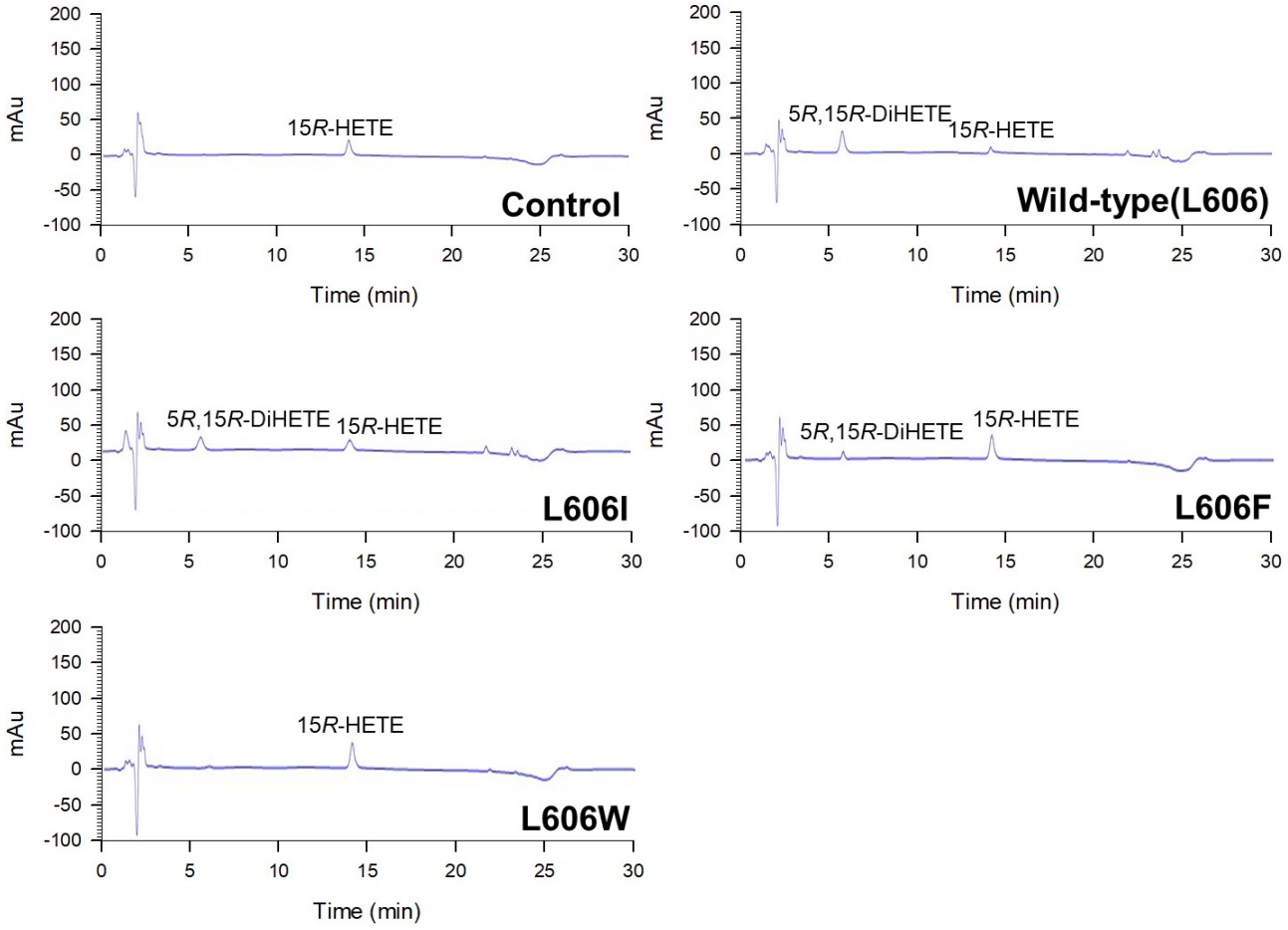

Fig. S29 Reverse-phase HPLC profiles of the products obtained from the conversions of ARA (**1**) and 15*R*-HETE (**3**) by the wild-type and variant LOXs at position 606 from *S. cellulosum*. The MonoHFAs and DiHFAs were analyzed using the Nucleosil C18 column. (A) HPLC profiles for reaction products obtained from the conversion of **1** by the wild-type and variant 15*R*-LOXs with **1** standard. The reactions were performed at 25 °C in 50 mM HEPES (pH 8.0) containing 1.0 mM **1**, 0.1 g/L cells, and 100 mM cysteine for 120 min. (B) HPLC profiles for the products obtained from the conversion of **1** by the variants at position 606. The reactions were performed at 25 °C in 50 mM HEPES (pH 8.0) containing 1.0 mM **1**, 0.1 g/L cells, and 100 mM cysteine for 120 min. (C) HPLC profiles for the products obtained from the conversion of 15*R*-HETE by the variants at position 606. The reactions were performed at 30 °C in 50 mM HEPES (pH 7.5) containing 0.5 mM **3**, 0.01 g/L of purified enzyme, and 100 mM cysteine for 30 min.

A

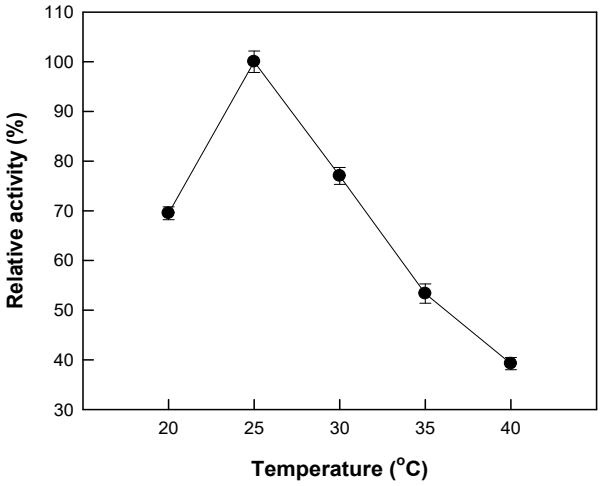

B

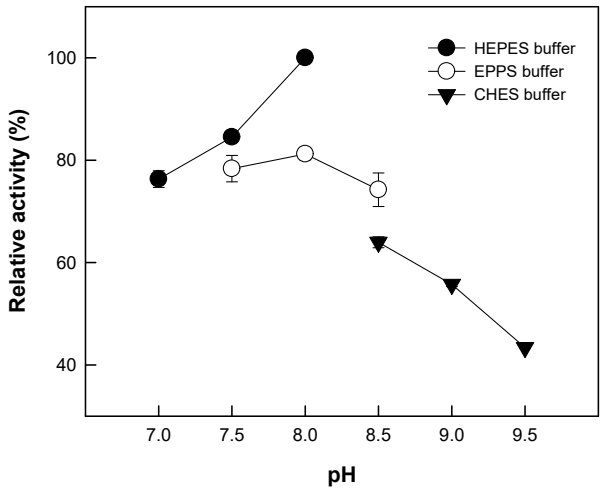

Fig. S30 Effects of temperature and pH on the biotransformation of ARA (**1**) into 15*R*-HETE (**3**) by *E. coli* expressing 15*R*-LOX from *S. cellulosum*. (A) Effect of temperature on the biotransformation of **1** into **3**. The reactions were performed in 50 mM HEPES (pH 8.0) buffer containing 1.0 g/L cells, 1.0 mM **1**, and 100 mM cysteine for 10 min by varying the temperature from 20 to 40 °C. (B) Effect of pH on the biotransformation of **1** into **3**. The reactions were performed in 50 mM HEPES, 50 mM EPPS, and 50 mM CHES buffers containing 1.0 g/L cells, 1.0 mM **1**, and 100 mM cysteine at 25 °C for 10 min by varying the pH from 7.5 to 9.5. Data represent the mean ± SD (n = 3) values.

A

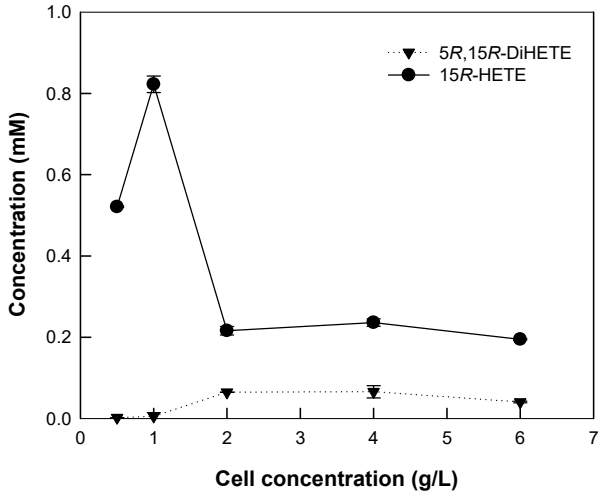

B

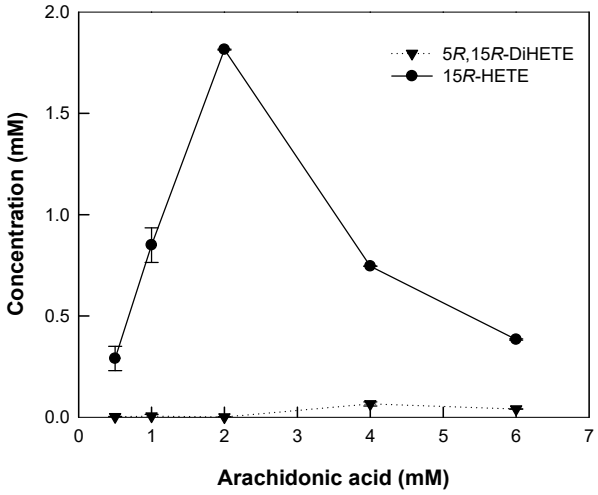

Fig. S31 Effects of cell and substrate concentration on the biotransformation of ARA (**1**) into 15*R*-HETE (**3**) by *E. coli* expressing engineered 15*R*-LOX (L606F variant). (A) Optimization on cell concentration for the biotransformation of **1** into **3**. The reactions were performed in HEPES (pH 8.0) buffer containing 1.0 mM **1**, 5.0 g/L SP825, and 100 mM cysteine for 30 min by varying the cell concentration from 0.5 to 6.0 g/L cells. (B) Optimization on substrate concentration for the biotransformation of **1** into **3**. The reactions were performed in HEPES (pH 8.0) buffer with cysteine containing 1.0 g/L cells, 5.0 g/L SP825, and 100 mM cysteine for 30 min by varying the substrate concentration from 0.5 to 6.0 mM. The optimal ratio of cells to substrate was 1:2 (g/L per mM). Data represent the mean ± SD (n = 3) values.

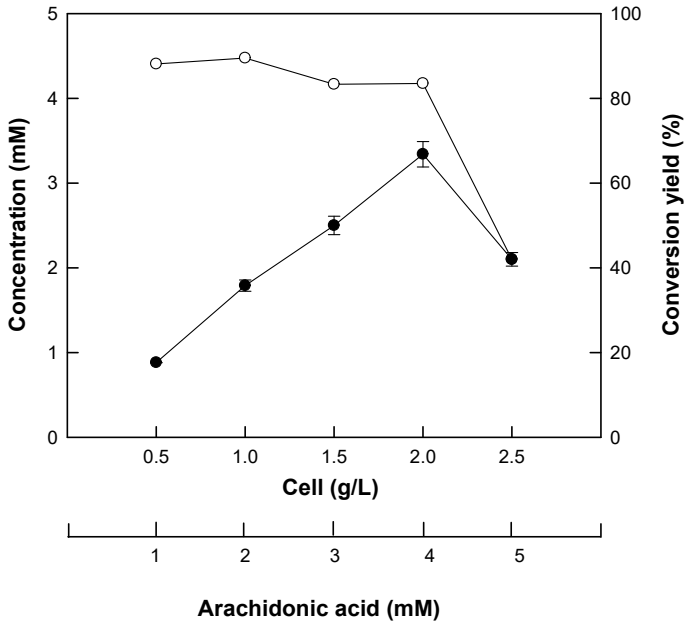

Fig. S32 Optimization of cell and substrate concentration on the biotransformation of ARA (**1**) into 15*R*- HETE (**3**) by *E. coli* expressing engineered 15*R*-LOX (L606F variant). The reactions were performed in a 100-mL flask containing 10 mL HEPES (pH 8.0) buffer supplemented with cells, substrate, and resin at the optimal ratio of 2:4:5 (g/L per mM per g/L) for 60 min by varying the concentrations of cells and **1** from 0.5 g/L and 1.0 mM to 2.5 g/L and 5.0 mM at the optimal ratio of 2.0 g/L to 4.0 mM. Data represent the mean ± SD (n = 3) values.

References

1 I. G. Lee, J. U. An, Y. J. Ko, J. B. Park and D. K. Oh, *Green Chem.* 2019, **21**, 3172-3181.

2 J. Lee, J. U. An, T. H. Kim, Y. J. Ko, J. B. Park and D. K. Oh, *Acs. Sustain. Chem. Eng.*, 2020, **8**, 16172-16183.

3 J. U. An, S. E. Kim and D. K. Oh, *Prog. Lipid. Res.*, 2021, **83**.

4 M. Jisaka, C. Iwanaga, N. Takahashi, T. Goto, T. Kawada, T. Yamamoto, I. Ikeda, K. Nishimura, T. Nagaya, T. Fushiki and K. Yokota, *Biochem. Bioph. Res. Co.*, 2005, **338**, 136-143.

5 J. Lee, J. U. An, T. H. Kim, Y. J. Ko, J. B. Park and D. K. Oh, *ACS Sustain. Chem. Eng.*, 2020, **8**, 16172-16183.

6 T. H. Kim, J. Lee, S. E. Kim and D. K. Oh, *Biotechnol. Bioeng.*, 2021, **118**, 3094-3104.

7 M. Jisaka, C. Iwanaga, N. Takahashi, T. Goto, T. Kawada, T. Yamamoto, I. Ikeda, K. Nishimura, T. Nagaya, T. Fushiki and K. Yokota, *Biochem. Biophys. Res. Commun.*, 2005, **338**, 136-143.